


The tidal prism as a dynamic response of a nonlinear harmonic system

Cite as: Phys. Fluids **35**, 017124 (2023); <https://doi.org/10.1063/5.0133390>

Submitted: 03 November 2022 • Accepted: 23 December 2022 • Published Online: 12 January 2023

 M. Petti,  S. Pascolo,  S. Bosa, et al.

COLLECTIONS

 This paper was selected as Featured



View Online



Export Citation



CrossMark

ARTICLES YOU MAY BE INTERESTED IN

[Dissipation-optimized proper orthogonal decomposition](#)

Physics of Fluids **35**, 015131 (2023); <https://doi.org/10.1063/5.0131923>

[Knowledge discovery with computational fluid dynamics: Supercritical airfoil database and drag divergence prediction](#)

Physics of Fluids **35**, 016113 (2023); <https://doi.org/10.1063/5.0130176>

[A phenomenological analysis of droplet shock-induced cavitation using a multiphase modeling approach](#)

Physics of Fluids **35**, 013312 (2023); <https://doi.org/10.1063/5.0127105>



Physics of Fluids

Special Topic: Paint and Coating Physics

Submit Today!

The tidal prism as a dynamic response of a nonlinear harmonic system

Cite as: Phys. Fluids **35**, 017124 (2023); doi: [10.1063/5.0133390](https://doi.org/10.1063/5.0133390)

Submitted: 3 November 2022 · Accepted: 23 December 2022 ·

Published Online: 12 January 2023



View Online



Export Citation



CrossMark

M. Petti,^{a)} S. Pascolo, S. Bosa, and N. Busetto

AFFILIATIONS

Dipartimento Politecnico di Ingegneria e Architettura, Università degli Studi di Udine, Udine, Italy

^{a)} Author to whom correspondence should be addressed: marco.petti@uniud.it

ABSTRACT

As known, the empirical relationship between the equilibrium cross-sectional area of a lagoon inlet and the tidal prism was intuited for the first time by LeConte [“Discussion on the paper, “Notes on the improvement of river and harbor outlets in the United States” by D. A. Watt,” Trans. ASCE **55**, 306–308 (1905).] and then formalized by O’Brien [“Estuary tidal prism related to entrance areas,” Civ. Eng. **1**(8), 738–739 (1931)]. This relationship requires knowledge of the tidal prism, which can be estimated either using the cubature method or the current data method [Jarrett, *Tidal Prism-Inlet Area Relationships* (Coastal Engineering Research Center, US Army Corps of Engineers, Fort Belvoir, VA, 1976)], both of which involve the execution of a number of experimental measurements. However, these methods, besides being very expensive, can only provide the prism value in the present condition and do not allow for predictions in the case of significant morphological changes, of both natural and anthropic origin, to the tidal inlet. On the other hand, the hydrodynamic relationship, which links the tidal prism to the product of the tidal range and the basin extension, can only give a coarse estimate of the prism, especially when the value of the tide outside the lagoon is considered. In this work, we propose a simple hydrodynamic relationship based on the dynamic response of a nonlinear harmonic system. This is a relationship that requires the calibration of a single physically based parameter. Through this relationship, knowing the geometric characteristics, the bottom friction of the inlet channel, the surface of the basin, and the tide amplitude in the open sea, it is possible to estimate the tidal prism. The application of this relationship to real cases shows a good agreement with the experimental data.

Published under an exclusive license by AIP Publishing. <https://doi.org/10.1063/5.0133390>

I. INTRODUCTION

In a lagoon system, adequate water exchange is fundamental for the survival of the environment because it guarantees the conditions of equilibrium necessary to safeguard the ecosystem. An important component of this exchange is the tide which, flowing through the inlets, introduces a large volume of water into the lagoon called the tidal prism.

For a basin, the tidal prism is defined as the total volume of water that flows through the inlet during half of the tidal cycle. Without significant external inputs or water exchanges between basins, the volume entering during the flood phase coincides with the outgoing volume in the ebb phase.

LeConte (1905) published the first morphological empirical relationship between the cross-sectional area of a tidal inlet and the tidal prism for harbor entrances on the Pacific coast,

$$\Omega = kP^\alpha \quad (1)$$

where, in SI unit, $k = 1.083 \cdot 10^{-4} \text{ m}^{-1}$ and $\alpha = 1$ for unprotected entrances and $k = 1.411 \cdot 10^{-4} \text{ m}^{-1}$ and $\alpha = 1$ for inner harbor

entrances. In the relationship (1), Ω is the minimum cross-sectional flow area below the mean sea level, and P is the tidal prism corresponding to the tidal spring range. It is important to note that in the relationship (1), α is dimensionless and k has dimension $\text{m}^{2-3\alpha}$; therefore, the dimension of k depends on α . O’Brien (1931), still analyzing data from the Pacific coast, revised the coefficients k and α of the relationship (1), and considering tidal prism P corresponding to the diurnal or spring tidal range, he found $k = 9.015 \cdot 10^{-4} \text{ m}^{-0.55}$ and $\alpha = 0.85$. O’Brien himself considered the good agreement between the experimental data and the relationship (1) to be fortuitous as the size of the bottom material in the inlet channel was not taken into account, inlets with or without jetties followed the same curve, and the tidal prism was computed by means of the hydrodynamic relationship,

$$P = 2a_m A, \quad (2)$$

where a_m is the tidal amplitude and A is the basin area relative to the inlet. In this regard, O’Brien mentioned the case of the “Fire Island Inlet,” where the tidal excursion within the lagoon is significantly lower than outside, and suggested calculating the prism either through

a detailed sum of all the contributions of the lagoon sub-areas (cubature method), taking into account the relative excursions and phase delays, or through a measurement of the water flow in the inlet channel (current data method). O'Brien concluded that the good agreement of the relationship (1) with the experimental data was conditioned by the limited amount of data analyzed, certain that an expansion of the series would have highlighted the perplexities cited.

O'Brien (1969) expanded the investigation analyzing the behavior of 28 lagoon inlets: nine on the Atlantic coast of the United States, 18 on the Pacific coast, and one on the Gulf. Among the 28 inlets, eight were without jetties, three with one jetty, and 17 with two jetties. Through a linear regression, he found the values $k = 6.562 \cdot 10^{-5} \text{ m}^{-1}$ and $\alpha = 1$ for the eight inlets without jetty and for prisms P ranging between $9.47 \cdot 10^6$ and $3.54 \cdot 10^9 \text{ m}^3$. Instead, for the 17 inlets with two jetties and with prisms in the interval $3.23 \cdot 10^5 - 1.08 \cdot 10^9 \text{ m}^3$, the values of $k = 9.015 \cdot 10^{-4} \text{ m}^{-0.55}$ and $\alpha = 0.85$ found in 1931 were confirmed. For the three inlets with only one jetty, O'Brien simply stated that the sections were included in the fields defined with the two previous curves.

Jarrett (1976) extended O'Brien's analysis to 108 inlets, again in the United States, dividing them into three main categories: without jetties, one jetty, or two jetties. Within each category, the inlets were further separated into groups corresponding to the three coasts: Pacific coast, Atlantic coast, and Gulf coast; the aim was to analyze data with similar hydraulic and morphological characteristics. This subdivision highlighted how, for each inlet type and for each coast, there were different values of k and α , varying between $k = 8.950 \cdot 10^{-6} \text{ m}^{-0.58}$ and $k = 1.922 \cdot 10^{-4} \text{ m}^{-0.55}$ and $\alpha = 0.85 - 1.10$. Jarrett concluded that, despite the subdivision into different types of inlets and the subdivision made by coast to take into account the different tidal fluctuations, the results obtained did not suggest changes to O'Brien's original relationships.

Several studies providing a theoretical background of the relationship (1) have been suggested (Escoffier, 1940; Krishnamurthy, 1977; Marchi, 1990; and Hughes, 2002), all of which are based on the condition of dynamic equilibrium reached when the bottom shear stress equals the critical threshold of incipient movement. These studies, based on the assumption of a logarithmic velocity profile, analyze the head losses across the channel as a function of the flow rate, and each of them provides a theoretical formula for both k and α . The relationships are distinguished by a different way of calculating the resistances (Engelund and Hansen, 1967; Keulegan, 1967; Escoffier, 1977; van de Kreeke, 1990; and D'Alpaos *et al.*, 2010); however, all agree on the dependence of k on the tidal period, the bottom friction, the channel width, and its cross-sectional area. Concerning the α exponent, Krishnamurthy (1977) found $\alpha = 1$, Marchi (1990) $\alpha = 6/7$, and Hughes (2002) $\alpha = 8/9$.

Stive *et al.* (2011) theoretically showed how a unique relationship (1) should be expected for clusters of inlets that are phenomenologically similar (i.e., fairly similar hydrodynamic and morphological conditions), and that the exponent α in the relation (1) should be larger than 1. However, the comparison with data available to date does not clearly support this theoretical result. Stive *et al.* (2011) stated that available datasets may not be sufficiently reliable to verify his theoretical finding due to the violation of the condition of phenomenological similarity, and possibly also due to the violation of the initial definitions given by O'Brien (1969) in estimating the tidal prism. Steve

considered this last aspect very important because slightly different values of α result in significantly variable values for the equilibrium cross-sectional area of the tidal inlet.

All attempts to theoretically substantiate the relationship (1) take into consideration important factors such as the tidal oscillations range, the possible action of the wave motion, the granulometry of the sediments, the presence of jetties, and other morphological components, but perhaps the same attention was not paid to the estimation of the tidal prism. Starting from O'Brien (1931) and (1969) and Jarrett (1976) in all of the works, the importance of calculating the tidal prism correctly is highlighted and often ends with a discussion about the advantages and disadvantages of an estimate made with the "cubature method" or the "current data method" (Jarrett, 1976). The relationship (1), determined on a wide experimental basis, is often used to obtain an estimate of the prism, but it does not provide considerations about the geometric and hydrodynamic variables that can affect the prism value. Alternatively, some theoretical approaches, based on the one-dimensional shallow water momentum equation, have been proposed in order to improve the understanding of the phenomenon, albeit with some necessary simplifications. For instance, Dean (1971) neglects the inertial term and linearizes the dissipative term, Mehta and Özsoy (1978) linearize the dissipative term using a first-order series expansion, and Larson *et al.* (2020) neglect the inertial term.

In addition, the relationship (1) is often used to estimate the prism, assuming that the inlet is already in an equilibrium state; however, this is not always the case (Powell *et al.*, 2006; Petti *et al.*, 2020; 2021). For example, when a human intervention or a particular perturbation changes the equilibrium condition, it can take tens of years to reach a new condition that is not necessarily the same. In these cases, it is important to know the hydrodynamic law that governs the dependence of the prism on the geometric and dynamic characteristics of the basin and the inlet because the new condition of morphological equilibrium is determined by the intersection of this law with the morphological relationship (1). Of course, it is always possible to use a numerical modeling (Helsby *et al.*, 2008; Umgiesser *et al.*, 2004; van der Wegen *et al.*, 2010; and Umgiesser *et al.*, 2015), however, having a simple hydrodynamic relationship which, though approximate, allows for quick evaluations can be very useful. This becomes very important if we consider that morphological changes of the lagoon inlets can have direct effects on the economic and technological resources used to guarantee their hydraulic efficiency and the navigability of the main channel. In this sense, it can be helpful to have a quick and easy tool available for the preliminary phase of a design or for small-scale studies.

The hydrodynamic relationship (2) can be used, as a first estimate of the prism, considering the external tidal amplitude and the basin extension, neglecting the propagation effects, as if the tide is instantaneously distributed within the basin, the tidal amplitude is the same throughout the basin. Therefore, as the basin area increases for an assigned tide, the prism would also linearly increase; however, some authors have found another behavior. In fact, recently, Reef *et al.* (2020), using a numerical approach, have shown that when the characteristic size of the lagoon basin increases, the tidal prism tends to an asymptotic value. Petti *et al.* (2021), again using a numerical approach, found the same behavior, highlighting how the prism tends to an asymptotic value both when the surface of the basin grows and when the cross-sectional

area of the inlet increases, in both cases with the same tidal amplitude.

With the aim of identifying a simple hydrodynamic relationship for the estimation of the tidal prism, this work proposes an approach based on the dynamic response of a nonlinear harmonic system. The aim is not to discuss a new morphodynamic law but to look for a simple hydrodynamic relationship that allows the prism to be calculated in a relatively simple way.

In the first part of the work, starting from the complete 1D momentum equation that governs the tidal prism, the nonlinear aspects of the problem are analyzed in a dynamic key. Subsequently, on the basis of the results obtained, a new formula is proposed for the calculation of the tidal prism, of relatively simple use, which requires the calibration of a single physically based parameter. Continuing, therefore, with the calibration of this parameter using the results of a 2DH model applied to a simple basin, we proceed with a verification of the reliability of the formula, applying it to lagoon basins in Italy, in the north of the Adriatic Sea, and to the Fire Island Inlet basin in the United States. Finally, a discussion of the results obtained is presented.

II. THE “INLET-BASIN” SYSTEM

A system consisting of a lagoon inlet and its basin can be seen as a nonlinear damped forced harmonic oscillator and its tidal prism as the dynamic response to such a system. To show this, we refer to the simplified lagoon system shown in Fig. 1(a) and to a system of Cartesian axes leaning on the still water level (SWL).

Starting from the “tide offshore,” the momentum equation across the lagoon inlet may be written as

$$\eta_m - \eta = \frac{L}{g} \frac{dU}{dt} + \frac{\xi_{eq}}{2g} U|U| + \frac{|U|U}{2g} + \frac{\xi_{en}}{2g} U|U| + \frac{L}{k_s^2 R^{4/3}} U|U| + \frac{\xi_{ex}}{2g} U|U|, \tag{3}$$

where η_m is the offshore tidal level, η is the tidal level near the exit channel (lagoon side), L is the inlet length, g is the gravity acceleration, t is the time, R is the channel hydraulic radius, U is the

instantaneous average inlet velocity, k_s is the Gauckler–Strickler coefficient, and ξ_{en} and ξ_{ex} are the entrance-loss and exit-loss coefficients, respectively. In transitional environments, such as lagoon inlets, the exchange between salt water and fresh water can generate exchange flows, which may have consequences on the driving mechanism of circulation within estuaries (De Falco *et al.*, 2021). However, in order to propose simple relationships, this aspect has been neglected in the present study. Tide offshore means measured at a distance such as to make the channeling effects due to the inlet negligible; ξ_{eq} is a coefficient that takes into account bed friction dissipations near the inlet entrance. To better understand this concept, the following considerations are important.

With reference to Fig. 1(b), we follow the tidal flow that starts from the open sea and enters the lagoon through the inlet. During this phase, as the flow approaches the inlet, a channeling process takes place (Fig. 2), which involves a progressive increase in speed. Therefore, it is natural to expect that near the inlet, the tide level will lower both following a transformation of potential energy into kinetics [third term of right-hand side of Eq. (3)] and due to a head loss caused by bed friction near the inlet entrance. To take into account the latter, it is assimilated to an equivalent loss $\xi_{eq}U|U|/(2g)$, where the coefficient ξ_{eq} is proportional to the distance of exhaustion of the phenomenon of channeling before the entrance and inversely proportional both to the sea bottom roughness and to the water depth. Following the path of the tidal flow, it suffers an entrance loss $\xi_{en}U|U|/(2g)$, a head loss due to channel friction $LU|U|/(k_s^2R^{4/3})$, and an exit loss $\xi_{ex}U|U|/(2g)$. Finally, immediately after exiting the channel (lagoon side), since the channeling effect does not immediately extinguish, it is reasonable to expect the speed to remain constant for a short distance and still equal to U . Consequently, the level can be considered constant, at least around the inlet [Fig. 1(b)].

Let us introduce

$$\xi = \xi_{en} + \xi_{ex} + \xi_{eq}. \tag{4}$$

Eq. (3) may be rewritten as

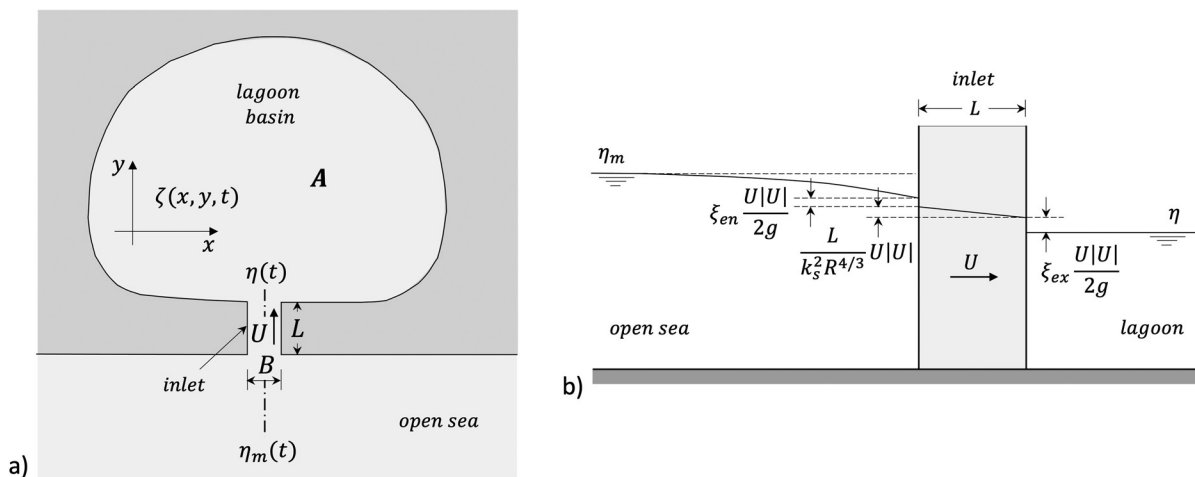


FIG. 1. (a) Lagoon inlet-basin system; (b) level losses between the offshore tide and the tide in the lagoon near the channel exit.

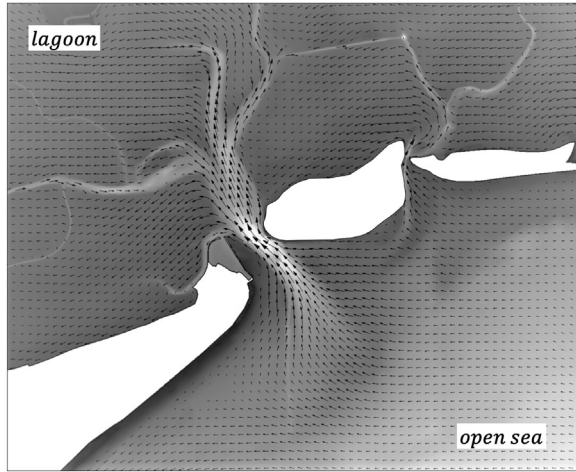


FIG. 2. Example of channelling effect near an inlet.

$$\eta_m - \eta = \frac{L dU}{g dt} + \left(\frac{L}{k_s^2 R^{4/3}} + \frac{\xi}{2g} + \frac{1}{2g} \right) |U|U. \quad (5)$$

In the ebb phase, the phenomenon is reversed.

The 1D approach (5), as well as being simple, is very interesting as it can provide information on the nonlinear behavior of the inlet-basin system, an aspect that allows us to estimate the tidal prism by taking into account the main geometric and dynamic characteristics of the lagoon, as illustrated below.

Concerning the mass balance of the inlet-basin system, at a given instant of time t , we have

$$U\Omega = \frac{dV}{dt}, \quad (6)$$

where dV/dt represents the volume gradient introduced into the lagoon through the inlet. If the surface of the basin is relatively large, the volume dV introduced at a given instant of time t does not spread immediately to all points of the lagoon but requires a certain time τ . Supposing to consider a “point” inside the basin where it is possible to measure the spatially averaged water level oscillation $\bar{\eta}$, we may write

$$dV(t) = A d\bar{\eta}(t + \tau), \quad (7)$$

with A being the hydrological surface of the basin,

$$\bar{\eta}(t') = \frac{1}{A} \int_A \zeta(x, y, t') dA, \quad (8)$$

the spatially averaged water level (Gao and Collins, 1994), and $\zeta(x, y, t')$ the tidal level at each point of the lagoon in the generic instant of time t' [Fig. 1(a)]. The hydrological surface is defined here as the liquid surface of the basin below the mean sea level.

In terms of $\bar{\eta}$, the continuity equation (7) may be rewritten as

$$U(t) = \frac{A}{\Omega} \frac{d\bar{\eta}(t + \tau)}{dt}, \quad (9)$$

where Ω is the mean cross-sectional flow area below mean sea level of the inlet channel.

Taking into account (4), combining Eqs. (9) and (3), after a few simple steps, we obtain

$$\begin{aligned} \frac{d^2 \bar{\eta}(t + \tau)}{dt^2} + \frac{A}{\Omega} \left(\frac{g}{k_s^2 R^{4/3}} + \frac{\xi}{2L} + \frac{1}{2L} \right) \left| \frac{d\bar{\eta}(t + \tau)}{dt} \right| \frac{d\bar{\eta}(t + \tau)}{dt} \\ + \frac{\Omega g}{AL} \eta(t) = \frac{\Omega g}{AL} \eta_m(t). \end{aligned} \quad (10)$$

Note that $\bar{\eta}$ is estimated at time $t + \tau$, while η and η_m are estimated at time t . The time lag τ depends on the propagation times of the tide in the lagoon.

Let us introduce

$$\omega_N = \sqrt{\frac{\Omega g}{AL}} \quad (11)$$

and

$$\gamma = \frac{A}{\Omega} \left(\frac{g}{k_s^2 R^{4/3}} + \frac{\xi}{2L} + \frac{1}{2L} \right), \quad (12)$$

changing the origin of times for convenience, Eq. (10) may be rewritten as

$$\frac{d^2 \bar{\eta}(t)}{dt^2} + \gamma \left| \frac{d\bar{\eta}(t)}{dt} \right| \frac{d\bar{\eta}(t)}{dt} + \omega_N^2 \eta(t - \tau) = \omega_N^2 \eta_m(t - \tau). \quad (13)$$

The term $\omega_N = \sqrt{\Omega g / (AL)}$ defines the oscillation mode known in the literature as Helmholtz or pumping mode, the typical angular frequency of an enclosed basin characterized by a periodic mass exchange with the sea through the inlet and by a spatially uniform elevation change within the basin (Bruun, 1978).

In order to have an estimate of the tidal time lag τ , we can approximate the basin with a semicircular shape having radius $r_0 = \sqrt{2A/\pi}$. Assuming, close to the lagoon side inlet, the sinusoidal tide

$$\eta(t) = a_l \sin(\omega t), \quad (14)$$

the mean level $\bar{\eta}$ results as

$$\bar{\eta} = \frac{2}{r_0^2} \int_0^{r_0} a_l \sin(\omega t - kr) r dr \quad (15)$$

being

$$k = \frac{\omega}{c_l}, \quad (16)$$

the wave number of the tide oscillation, r is the distance of the tidal front from the inlet, and c_l is the phase velocity of the tidal wave. Integrating (15), we obtain

$$\bar{\eta} = a_l \frac{2c_l^2}{\omega^2 r_0^2} \left[\sin\left(\omega t - \omega \frac{r_0}{c_l}\right) + \omega \frac{r_0}{c_l} \cos\left(\omega t - \omega \frac{r_0}{c_l}\right) - \sin(\omega t) \right], \quad (17)$$

a relationship that may be rewritten as

$$\bar{\eta} = k_r a_l \sin\left[\omega\left(t - \frac{2r_0}{3c_l}\right)\right], \quad (18)$$

where k_r is a reduction coefficient.

Let us introduce

$$\tau = \frac{2r_0}{3c_l}, \tag{19}$$

and the relationship (18) becomes

$$\bar{\eta} = k_r a_l \sin[\omega(t - \tau)] = k_r \eta(t - \tau), \tag{20}$$

that is, compared to the η oscillation near the inlet (lagoon side), the mean level $\bar{\eta}$ is reduced by a factor k_r and delayed by a time τ . Comparing the Eqs. (17) and (18), for a basin surface $A = 250 \cdot 10^6 \text{ m}^2$, we have $k_r = 0.98$, and for smaller surfaces, k_r increases until the maximum value 1. For larger surface values, the coefficient tends to decrease, but generally very extensive coastal lagoons are characterized by multiple inlet systems, and therefore, $k_r = 0.98$ can be considered with good approximation as a minimum value.

Therefore, assuming a coefficient $k_r \cong 1$, Eq. (13) may be rewritten as

$$\frac{d^2 \bar{\eta}(t)}{dt^2} + \gamma \left| \frac{d\bar{\eta}(t)}{dt} \right| \frac{d\bar{\eta}(t)}{dt} + \omega_N^2 \bar{\eta}(t) = \omega_N^2 \eta_m(t - \tau). \tag{21}$$

By forcing the system with the sinusoidal tide offshore

$$\eta_m(t) = a_m \sin(\omega t), \tag{22}$$

the differential equation that describes the “lagoon inlet-basin” system becomes

$$\frac{d^2 \bar{\eta}(t)}{dt^2} + \gamma \left| \frac{d\bar{\eta}(t)}{dt} \right| \frac{d\bar{\eta}(t)}{dt} + \omega_N^2 \bar{\eta}(t) = \omega_N^2 a_m \sin[\omega(t - \tau)], \tag{23}$$

where γ , defined with (12), is a coefficient that takes into account all the distributed and concentrated losses across the lagoon inlet. Equation (23) describes a nonlinear damped harmonic oscillator forced by the tidal oscillation $\eta_m(t - \tau)$ (Shin and Hammond, 2008).

Equation (23), referring to η instead of $\bar{\eta}$, has been solved in an approximate way by several authors, some of them have linearized the dissipative term using different techniques, and others have neglected the inertial term (e.g., Dean, 1971; Mehta and Özsoy, 1978; Mei, 2003; and Larson et al., 2020). The approximate method we propose in this paper, aimed at estimating the tidal prism, minimizes the error of the $\bar{\eta}$ estimate and, in addition, taking into account $\bar{\eta}$ instead of η , also considers the energy transformations and dissipations before the entrance. Before illustrating the method, it is important to define the degree of nonlinearity of the system (23), and a possible way could be the following.

Introducing the dimensionless variables

$$\bar{\eta}^* = \frac{\bar{\eta}}{a_m}, \quad t^* = \omega t \quad \text{e} \quad \tau^* = \omega \tau, \tag{24}$$

the offshore tide results as

$$\eta_m^*(t^*) = \sin(t^*), \tag{25}$$

while the differential equation (23) can be rewritten as

$$\begin{aligned} \omega^2 \frac{d^2 \bar{\eta}^*(t^*)}{dt^{*2}} + \gamma a_m \omega^2 \left| \frac{d\bar{\eta}^*(t^*)}{dt^*} \right| \frac{d\bar{\eta}^*(t^*)}{dt^*} + \omega_N^2 \bar{\eta}^*(t^*) \\ = \omega_N^2 \sin(t^* - \tau^*) \end{aligned} \tag{26}$$

or

$$\begin{aligned} \left(\frac{\omega}{\omega_N} \right)^2 \frac{d^2 \bar{\eta}^*(t^*)}{dt^{*2}} + \gamma a_m \left(\frac{\omega}{\omega_N} \right)^2 \left| \frac{d\bar{\eta}^*(t^*)}{dt^*} \right| \frac{d\bar{\eta}^*(t^*)}{dt^*} + \bar{\eta}^*(t^*) \\ = \sin(t^* - \tau^*). \end{aligned} \tag{27}$$

Analyzing the structure of Eq. (27), it is easy to see how the nonlinearities of the inlet-basin system are governed by the parameter,

$$E_m = \gamma a_m \left(\frac{\omega}{\omega_N} \right)^2, \tag{28}$$

which hereafter will be called the nonlinearity parameter of the inlet-basin system. Of course, small values of E_m imply weak nonlinearities, whereas high values imply strong nonlinearities.

It is interesting to note that if

$$\left(\frac{\omega}{\omega_N} \right)^2 \ll 1 \quad \text{and} \quad E_m = O(1), \tag{29}$$

where $O()$ means the same order of magnitude, and the inertial term of the system (27) is negligible (e.g., Dean, 1971; Larson et al., 2020).

Furthermore, if

$$E_m \ll 1, \tag{30}$$

the system behaves like a harmonic oscillator without damping.

Finally, if

$$\left(\frac{\omega}{\omega_N} \right)^2 \ll 1 \quad \text{and} \quad E_m \ll 1, \tag{31}$$

the mean tidal amplitude in the lagoon coincides, except for a shift in time, with the tidal amplitude offshore.

As an example, Fig. 3 shows a numerical solution for the differential equation (27) obtained with a simple second order finite difference numerical method.

Associating to the solution $\bar{\eta}^*$, the amplitude a_l^* is defined as

$$a_l^* = \frac{\bar{\eta}_{max}^* - \bar{\eta}_{min}^*}{2}, \tag{32}$$

and a phase lag φ measured as the dimensionless temporal distance between the tidal peak offshore η_m^* and the tidal peak of the mean level $\bar{\eta}^*$ (Fig. 3). It is possible to obtain the curves $H_n(\gamma a_m, \omega/\omega_N) = a_l^*$ and $\varphi_n(\gamma a_m, \omega/\omega_N)$, shown in Figs. 4(a) and 4(b), respectively, called amplitude response and phase lag of the system (27). It is useful to specify that the amplitude response is independent of the time lag τ^* , and if $\tau^* > 0$, the overall phase lag is $(\tau^* + \varphi)$.

To be thorough, in Fig. 5, the amplitude response is depicted as a function of γa_m and of the dimensionless variable $\omega_N/\omega = \sqrt{\Omega g/(AL\omega^2)}$, useful for linking H_n to the geometric characteristics of both the inlet and the basin.

If, on the one hand, the numerical integration of the system (27) is the most formally correct way, on the other hand, it does not lend itself to a very flexible use; for this reason, it may be useful to search for approximate solutions that are easy and can be applied quickly. One way may be to linearize the dissipative term of the system (27) as follows.

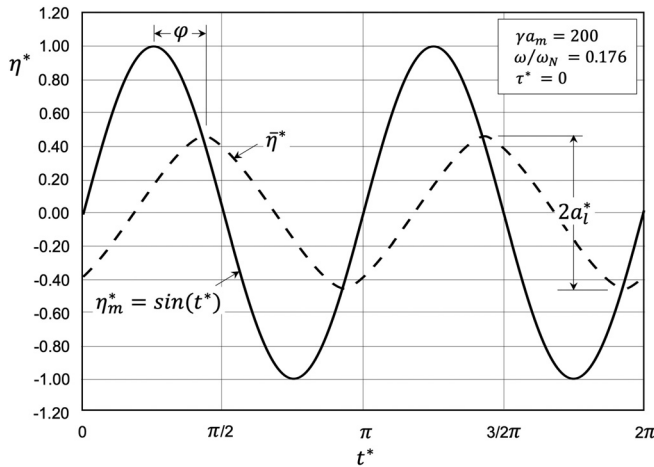


FIG. 3. Example of numerical solution of the nonlinear system of system (27).

We assume

$$\left| \frac{d\bar{\eta}^*(t^*)}{dt^*} \right| \approx \frac{1}{2} \frac{d\bar{\eta}^*(t^*)}{dt^*} \tag{33}$$

consistent with the variability between 0 and 1 of the term $|d\bar{\eta}^*(t^*)/dt^*|$. The error introduced with this approximation will be quantified shortly.

Combining Eqs. (33) and (27), we find

$$\left(\frac{\omega}{\omega_N}\right)^2 \frac{d^2\bar{\eta}^*(t^*)}{dt^{*2}} + \frac{\gamma a_m}{2} \left(\frac{\omega}{\omega_N}\right)^2 \frac{d\bar{\eta}^*(t^*)}{dt^*} + \bar{\eta}^*(t^*) = \sin(t^* - \tau^*) \tag{34}$$

equation describing a forced linear damped harmonic system.

With reference to (34), setting $\tau^* = 0$ and defining

$$\lambda = \frac{\gamma a_m}{4} \left(\frac{\omega}{\omega_N}\right), \tag{35}$$

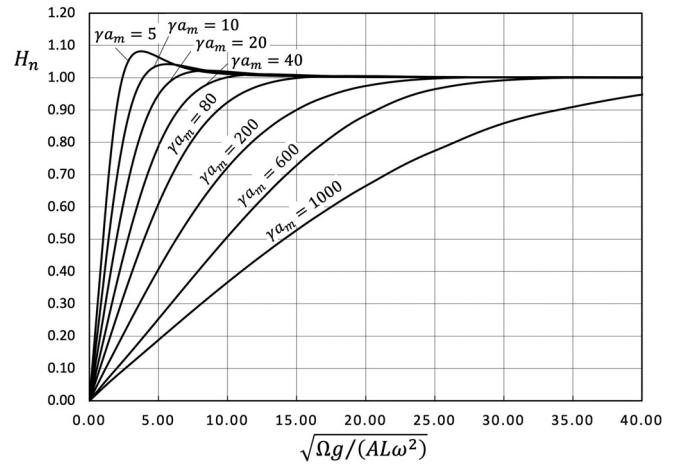
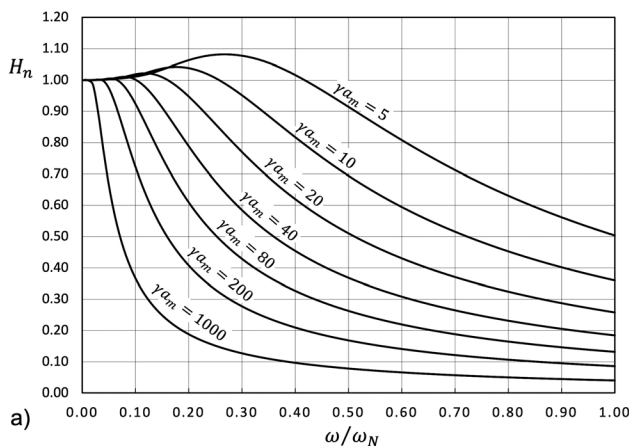


FIG. 5. Amplitude response of the nonlinear system (27) vs $\sqrt{\Omega g/(AL\omega^2)}$ for values $\gamma a_m = [5, 1000]$.

different solutions of the system can be found, depending on whether λ is greater, equal, or less than 1. However, in all cases, the amplitude response is (see Appendix)

$$H_I(\gamma a_m, \omega/\omega_N) = \frac{1}{\sqrt{\left[1 - \left(\frac{\omega}{\omega_N}\right)^2\right]^2 + \left[\frac{\gamma a_m}{2} \left(\frac{\omega}{\omega_N}\right)^2\right]^2}}. \tag{36}$$

Naturally, the linear approximation (33) does not satisfy the whole domain of ω/ω_N values, and in fact if, for example, for $\gamma a_m = 100$, we compare the numerical solution of the complete differential Eq. (27) with the linear solution (36), we obtain the result shown in Fig. 6. As you can see, when increasing ω/ω_N , the linear solution diverges, and in particular, for $\gamma a_m = 100$, it begins to do so for $\omega/\omega_N > 0.15$.

With the aim of finding a relationship easily usable in real applications even for higher ω/ω_N values, the following semi-empirical relationship is proposed:

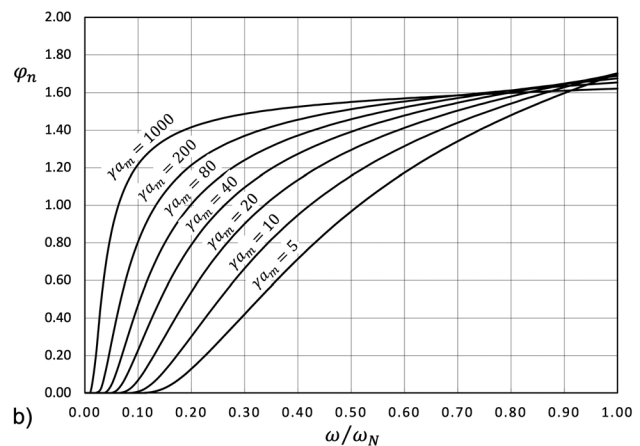


FIG. 4. Nonlinear system (27): (a) amplitude response and (b) phase lag response for values $\gamma a_m = [5, 1000]$ and $\tau^* = 0$.

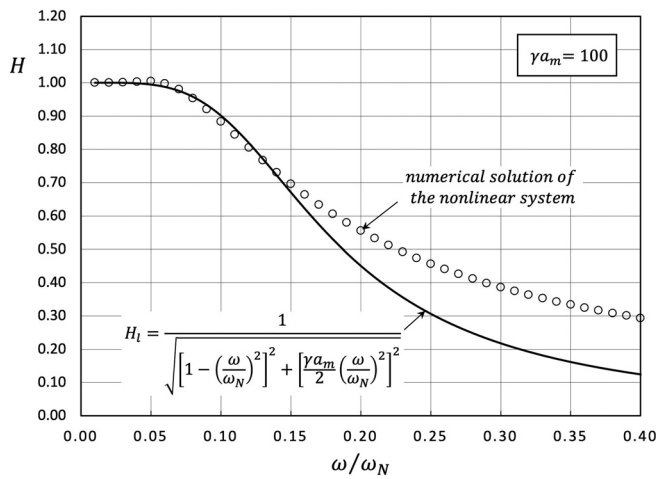


FIG. 6. Trend of the H response vs ω/ω_N : comparison between linear and nonlinear (numerical) solution in the case of $\gamma a_m = 100$.

$$H(\gamma a_m, \omega/\omega_N) = \frac{1}{\sqrt{\left[1 - \left(\frac{\omega}{\omega_N}\right)^2\right]^\alpha + \left[\frac{\gamma a_m}{2} \left(\frac{\omega}{\omega_N}\right)^2\right]^\beta}}, \quad (37)$$

with α and β coefficients to be determined numerically. To do this, the relative percentage error is defined as

$$\varepsilon_H\% = 100 \cdot \max \left| \frac{H - H_n}{H_n} \right|, \quad (38)$$

where H_n is the numerical response [Fig. 4(a)], and we proceeded iteratively looking for the values of α and β that gave an error $\varepsilon_H\%$ less than or equal to the linear one. The survey was limited to the range $E_m \leq 44$, which was considered adequate to sufficiently represent any basin system.

At the end of the process, the α and β values shown in Table I and the two domains, linear and nonlinear, shown in Fig. 7(a) were identified. The separation curve of the two domains was obtained as the intersection of the two responses (37) having $(\alpha, \beta) = (2, 2)$ and $(\alpha, \beta) = (0, 1.125)$.

The phase lag φ , although important from the point of view of the system response, does not enter directly into the calculation of the tidal prism, as we will see shortly. For this reason, given the purposes of the present work, it is not treated further.

Returning to the example shown in Fig. 6, using the (37) with parameters $(\alpha, \beta) = (0, 1.125)$, the result depicted in Fig. 7(b) can be obtained.

Mehta and Özsoy (1978) starting from Eq. (13) expressed as a function of η (therefore without taking into account the time lag τ)

TABLE I. Values of α and β valid for $0 < \omega/\omega_N \leq 1$ and $E_m \leq 44$.

Range	Response	α	β
Linear	H_l	2	2
Nonlinear	H_{nl}	0	1.125

and, using dimensionless variables slightly different from those described in this work, linearized the dissipative term by means of a Fourier series interrupted at the first order, obtaining the solution

$$H_{mo}(\gamma a_m, \omega/\omega_N) = \frac{\left\{ \left[1 - \left(\frac{\omega}{\omega_N}\right)^2\right]^4 + \left[\frac{16}{3\pi} \gamma a_m \left(\frac{\omega}{\omega_N}\right)^2\right]^2 \right\}^{1/2} - \left[1 - \left(\frac{\omega}{\omega_N}\right)^2\right]^2}{\sqrt{\frac{1}{2} \left[\frac{16}{3\pi} \gamma a_m \left(\frac{\omega}{\omega_N}\right)^2\right]^2}}, \quad (39)$$

considered valid for any ω/ω_N ratio. In their approach, Mehta and Özsoy (1978) only considered the entrance and exit energy losses at the inlet and the bottom friction dissipations along the relative channel. In this sense, in order to obtain the H_{mo} response as a function of the dimensionless variables chosen in the present study, the entrance and exit energy losses have been rewritten, taking into account the contributions of the channeling mechanism, which includes the losses due to bottom friction dissipations near the inlet and the transformation of potential energy into kinetic energy. This means that the sum of the two coefficients ξ_{en} and ξ_{ex} has been replaced by the more general term $(\xi + 1)$.

Comparing the solutions (39) and (37), we obtain the outcomes shown in Fig. 8(a). It can be observed that the response H proposed in this paper tends to overestimate the numerical one H_n , while the one proposed by Mehta and Özsoy tends to underestimate it. To have a numerical comparison, the relative maximum percentage errors $\varepsilon_H\%$ were compared. The result for $\omega/\omega_N \leq 1$ (as expected in lagoon systems) and $E_m \leq 44$ is shown in Fig. 8(b). As can be seen, for $\gamma a_m > 8$, the relationship (37) gives an error smaller than that given by (39), less than 6% for $\gamma a_m \geq 10$. For $\gamma a_m = 8$, the two relations are equivalent, while for values of $\gamma a_m < 8$, the relationship (39) is better than (37).

III. TIDAL PRISM

The tidal prism, as known, is defined as

$$P = \int_{\Delta t} Q dt = \int_{\Delta t} U \Omega dt, \quad (40)$$

where Δt is the time in a tidal cycle in which $U > 0$, flood phase, or $U < 0$, ebb phase.

Using Eq. (9), you may also write

$$P = \int_{\bar{\eta}_{min}}^{\bar{\eta}_{max}} A d\bar{\eta} = A(\bar{\eta}_{max} - \bar{\eta}_{min}). \quad (41)$$

Recalling, in dimensional form, the definition of the tidal amplitude (32)

$$a_l = \frac{\bar{\eta}_{max} - \bar{\eta}_{min}}{2}, \quad (42)$$

you may also write

$$P = 2a_l A. \quad (43)$$

For the rest, we define

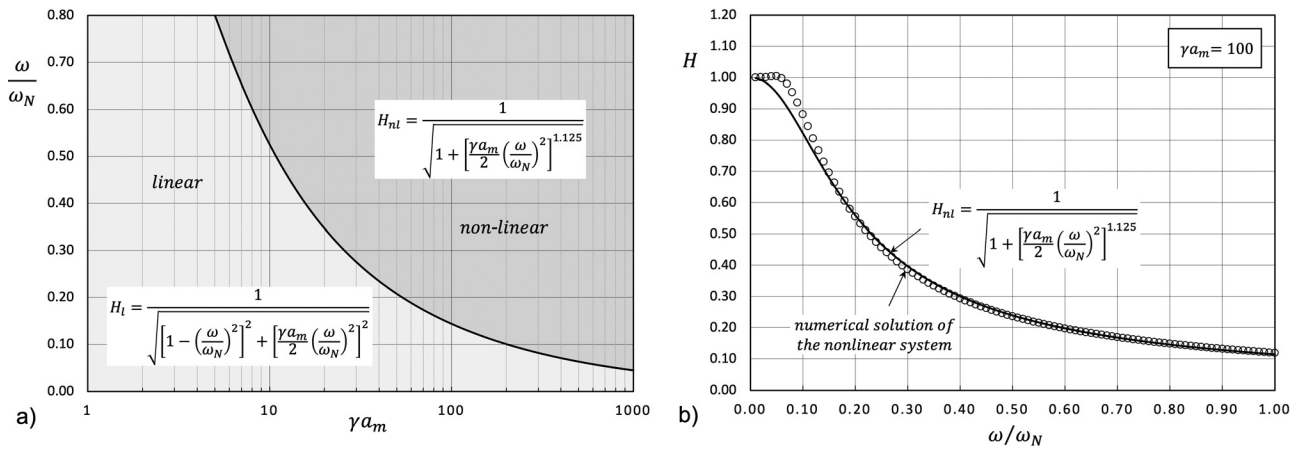


FIG. 7. (a) Field of validity of the linear (H_l) and nonlinear (H_{nl}) response H vs the parameters γa_m and ω/ω_N ; (b) trend of the H response vs the ω/ω_N ratio in the case $\gamma a_m = 100$.

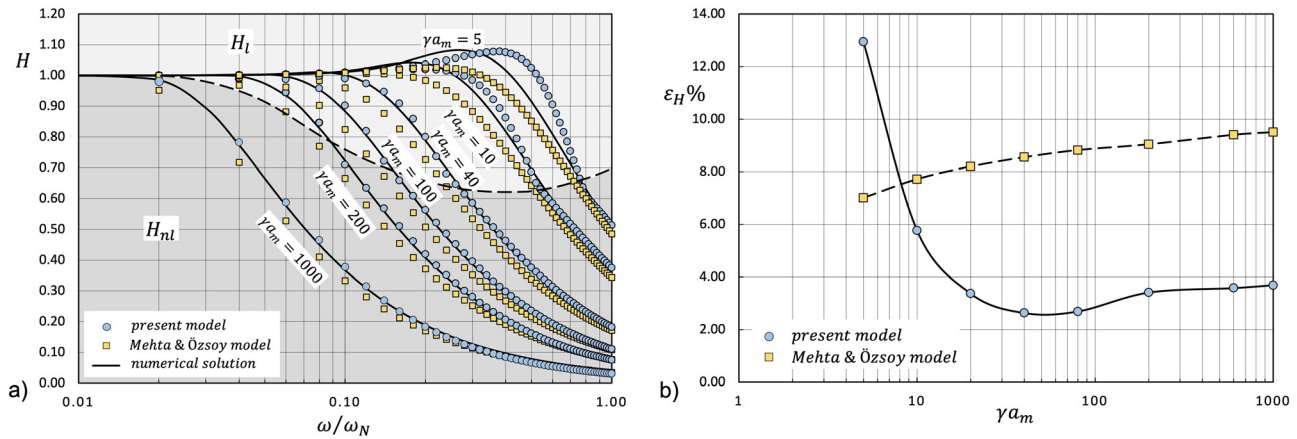


FIG. 8. (a) Comparison between the response H obtained with the relations (37) and (39) vs ω/ω_N and for $\gamma a_m = [5, 1000]$. The dashed line separates the validity fields of the linear (light gray) and nonlinear (dark gray) responses. (b) Maximum relative error percentage $\varepsilon_H\%$ vs γa_m in the range $0 < \omega/\omega_N \leq 1$ and for $E_m \leq 44$.

$$P_0 = 2a_m A, \tag{44}$$

the tidal prism that would occur if the amplitude of the mean tide level inside the lagoon coincides with that in the open sea [conditions (31)].

By dividing Eq. (43) with Eq. (44), we get

$$\frac{P}{P_0} = \frac{a_l}{a_m} = H, \tag{45}$$

consequently, the tidal prism $P^{(H)}$ in the range $0 < E_m \leq 44$, unless an error $|\varepsilon_H| \leq 3.7\%$, can be calculated with the relationship

$$P^{(H)} = 2a_m A H, \tag{46}$$

where H is given by Eq. (37), and the exponents α and β , for $\omega/\omega_N \leq 1$ and $E_m \leq 44$, are those shown in Table 1.

It is easy to see that if

$$\frac{\omega}{\omega_N} \ll 1 \quad \text{and} \quad E_m = \gamma a_m \left(\frac{\omega}{\omega_N}\right)^2 \ll 1, \tag{47}$$

the relationship (46) is reduced to Eq. (2), already used in the past to calculate the prism (O'Brien, 1931).

The dimensionless variables that affect the prism are ω/ω_N and γa_m [Eq. (37)], but while the former is easy to calculate, the latter can create some difficulties. The origin of the problem lies in the attribution of a value to the coefficient ζ included in γ . Recalling Eq. (12) and thinking about the typical characteristics of a lagoon inlet, it is not difficult to find that

$$\frac{\zeta}{2L} = O\left(\frac{g}{k_s^2 R^{4/3}}\right). \tag{48}$$

Even in some circumstances, for example, in the case of armed inlets, the losses associated with the coefficient ζ may exceed those distributed in the inlet. It follows that a correct estimate of this coefficient assumes a very important role in the estimation of the tidal prism, a role comparable, if not greater than the loss distributed in the channel.

The two ways to estimate the ζ coefficient are the experimental one, both in the field and in the laboratory, or the numerical one. In this work, the latter path has been followed.

IV. CALIBRATION OF THE COEFFICIENT ζ

In most of the works that use the morphological relationship (1), the difference between inlets with and without jetties is underlined. In the relationship proposed in this paper, this difference is reflected in the coefficient ζ , especially for the head loss before the inlet. This additional loss derives from a channeling process of the current that can involve a large area around the tidal inlet and during which the flow lines tend to concentrate and the current velocity progressively increases until it reaches the maximum value in correspondence with the inlet. In this paper, an initial estimate of the coefficient ζ is proposed by means of a numerical approach, in order to obtain a general formulation that can take into account the presence or absence of the jetties. Some numerical tests were carried out on a series of simplified basins with rectangular shape (Fig. 9). The main features of the computational domain derive from the numerical simulations performed by Petti et al. (2021), with the aim of understanding the effects on the tidal prism of some geometric and hydrodynamic characteristics of the tidal inlet, channel, and the lagoon basin.

For the basins, four surfaces $A = 25, 50, 100,$ and 200 km^2 (Fig. 9) with a constant depth $h_l = -1.2 \text{ m}$ were examined. Externally, a sufficiently large sea area was considered with a horizontal bottom having a depth $h_s = -7 \text{ m}$. The sea area and the basin were connected with a trapezoidal channel, having a depth $h_c = -7 \text{ m}$, an average width $B_c = 250 \text{ m}$, and a length $L_c = 250 \text{ m}$, gradually connected internally to the depth of the basin h_l . The scheme does not reproduce the natural network of channels separated from the tidal flats, typical of these transition environments (Fig. 2). The bed roughness and bottom height of these two features can be very different, with implications especially on current bed shear stress (Monti et al.,

TABLE II. Quantities used in simulations.

$\Omega \text{ (m}^2 \cdot 10^6\text{)}$	$L_c \text{ (m)}$	$R \text{ (m)}$	$a_m \text{ (m)}$	$T \text{ (h)}$
1750	250	5.81	0.4	12

2019; Dey et al., 2021; and Rathore et al., 2021). However, this particular aspect is not decisive in estimating losses near the inlet.

Eight tests were performed: four without jetties and four with jetties, two for each basin surface. For each test, the Ω section, length L_c , and hydraulic radius R of the channel as well as tidal amplitude and period offshore a_m and T were kept constant (Table II). The length L_j of the jetties, in the tests in which their presence was planned, was assumed to be equal to 1000 m. Regarding the Gauckler–Strickler roughness coefficient k_s , a constant value equal to $40 \text{ m}^{1/3} \text{ s}^{-1}$ was assumed at sea, in the channel and in the lagoon, which corresponds to the uniform value adopted by Petti et al. (2021), following Marchi’s approach (1990). Furthermore, this value was successfully used to carry out several simulations of the main hydrodynamic processes in the northern Adriatic nearshore, in Italy (Petti et al., 2018; 2020).

A numerical model, developed in-house, was used for the simulations; the model integrates the shallow water hydrodynamic equations in their two-dimensional form (2DH) through a finite volume technique. The adopted scheme has shock-capturing properties deriving from the application of the Riemann Harten-Lax-van Leer-Contact (HLLC) solver; the particular hydrostatic reconstruction of the variables also allows for the conservation of the C-property. A complete description of the model used is reported in Petti et al. (2018).

At the end of each simulation, the tidal prism $P^{(2DH)}$ was estimated as the integral of the flow rates flowing through the inlet [Eq. (40)] and the prism P_0 using the relationship (44). For each test, Table III shows the surface A , the prism P_0 , and the prism $P^{(2DH)}$ estimated both with and without jetties.

Subsequently, using the relationship (46), the value ζ was iteratively estimated using a stopping criterion based on the relative percentage error, defined as

$$\varepsilon_P\% = 100 \cdot \max \left| \frac{P^{(H)} - P^{(2DH)}}{P^{(2DH)}} \right|, \tag{49}$$

where $P^{(H)}$ is the prism estimated with the (46) and $P^{(2DH)}$ is the prism obtained with the numerical model. The stopping criterion

TABLE III. Prism P_0 and $P^{(2DH)}$ for each test.

	Test	$A \text{ (m}^2 \cdot 10^6\text{)}$	$P_0 \text{ (m}^3 \cdot 10^6\text{)}$	$p^{(2DH)} \text{ (m}^3 \cdot 10^6\text{)}$
Without jetties	S25	25	20	20.32
	S50	50	40	34.24
	S100	100	80	39.32
	S200	200	160	37.98
With jetties	S25M	25	20	20.00
	S50M	50	40	30.85
	S100M	100	80	33.15
	S200M	200	160	32.44

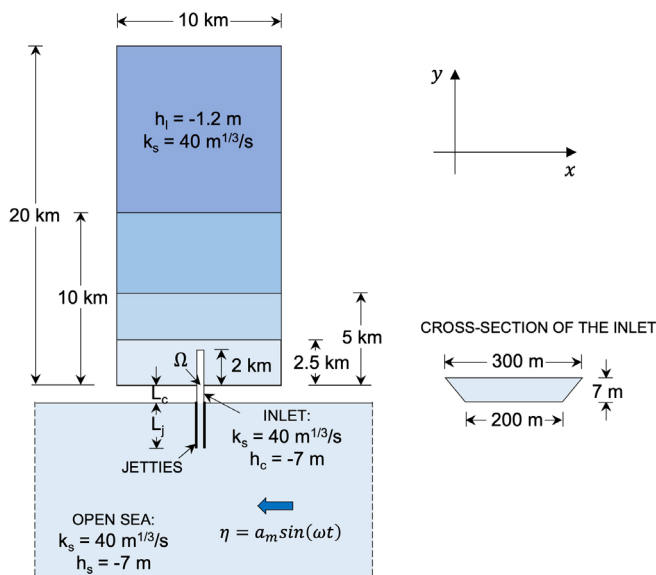


FIG. 9. Simplified basin scheme.

TABLE IV. Estimate of the coefficient ζ .

	Test	γa_m	ω/ω_N	λ	E_m	$P^{(2DH)}$ ($m^3 \cdot 10^6$)	ζ	$P^{(H)}$ ($m^3 \cdot 10^6$)	$\varepsilon_p\%$
Without jetties	S25	32.53	0.088	0.71	0.25	20.57	1.6	20.00	2.77
	S50	78.77	0.124	9.77	1.21	34.45	2.20	34.58	0.38
	S100	178.11	0.176	31.35	5.49	39.20	2.65	39.62	1.07
	S200	379.07	0.248	94.01	23.36	39.20	2.90	39.12	0.20
With jetties	S25M	9.90	0.196	1.94	0.38	20.32	2.10	20.40	0.39
	S50M	22.77	0.278	6.33	1.75	31.25	2.75	31.42	0.54
	S100M	50.11	0.393	16.69	7.72	33.30	3.25	33.98	2.04
	S200M	104.79	0.555	58.16	32.29	33.40	3.50	32.82	1.74

consisted of reaching a $\varepsilon_p\%$ error as small as possible and in any case less than the $\varepsilon_H\%$ error [Fig. 8(b)]. In the presence of jetties, the quantity $L = L_c + L_j$ was assumed as the length of the channel. The results are shown in Table IV.

Remembering that ζ is a coefficient that takes into account the head loss due to bed friction near the inlet entrance (ζ_{eq}), the head loss on entrance (ζ_{en}), and the loss on exit (ζ_{ex}), as a first approximation, it seems reasonable to assume that the coefficient ζ depends on the velocity U in the channel. Using the relationship (9) and the dimensionalization already seen, it is not difficult to show that

$$U = \frac{A\omega a_m}{\Omega} U^*, \tag{50}$$

where U^* is the dimensionless velocity of the current in the inlet. Using this result, it would appear useful to refer the trend of the coefficient ζ in function of the dimensionless variable $A\omega a_m/\Omega$, both in the presence and absence of jetties (Fig. 10).

To better understand the role played by the different head losses (near the inlet entrance, on entrance, and on exit), Fig. 11 shows the trend of the tide profiles along a longitudinal section of the inlet, in the instant of maximum tidal gradient during both flood and ebb phases.

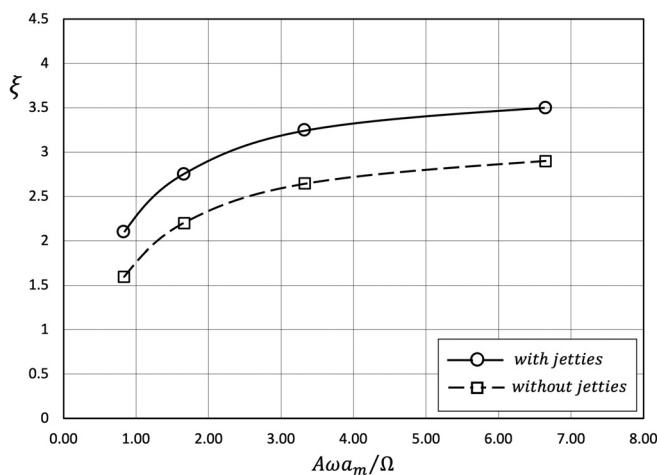


FIG. 10. Trend of the coefficient ζ vs the dimensionless variable $A\omega a_m/\Omega$ (a uniform Gauckler–Strickler coefficient $ks = 40 \text{ m}^{1/3} \text{ s}^{-1}$ has been assumed both in the open sea and the lagoon domain).

As you can see, in all cases, the difference at the inlet entrance $\Delta\eta = (\zeta_{eq} + 1)U|U|/(2g)$ is very significant. The lowering of the water level is partly due to the increase in current velocity and, therefore, in the relative kinetic energy, but the bottom friction dissipations seem to play the major role in the channeling process. Moreover, it can be observed that the level further decreases as the extension of the lagoon basin increases, for an assigned inlet cross section. This condition indicates a greater flow recall effect for larger basin surfaces. This result is clearly visible in the trend of the graphs in Fig. 10, which can be, therefore, assumed as an initial but general estimate of the coefficient ζ .

Furthermore, it is also interesting to observe how the profiles of the level exiting the inlet confirm the assumption made in writing the balance (3) of constant U , and consequently η constant near the inlet exit, both in the phase of the flood and ebb of tide. The profile inside the basin tends toward a uniform value, with the exception of a discontinuity, which is highlighted at the end of the channel that extends for 2 km from the inlet. Here, a reduction in the level takes place, due to the widening of the section of the current flow, which is no longer channelled.

V. APPLICATION TO REAL BASINS

A. Venice and Marano-Grado lagoons

As an initial check of relationships (46) and (37), it was decided to apply them to basins in the lagoons of Venice and Marano-Grado.

The lagoons of Venice and Marano-Grado are two large basins in the northern Adriatic Sea, the first is 550 km^2 and the second is 160 km^2 (Dorigo, 1965; Fontolan et al., 2007) (Fig. 12). Six inlets connect the Marano and Grado lagoon to the sea, from east to west: Primero, Grado, Morgo, Buso, S. Andrea, and Lignano; of these, Grado, Buso, and Lignano are the largest. In its present condition, there are two jetties on the inlets of Buso and Grado; before 1967, these did not exist. Three large inlets connect the Venice lagoon to the Adriatic Sea, from north to south: Lido, Malamocco, and Chioggia; all of them have had two long jetties since the 19th century. Both lagoons have an average water depth of about 1 m (Petti et al., 2018; Ungiesser et al., 2004).

In the northern Adriatic, the tides are semi-diurnal, and their average excursion measured over the last 30 years is 0.78 m in Grado and Trieste, and 0.73 m in Venice Lido and the Venice oceanographic tower. In the same period, the average interval measured for spring

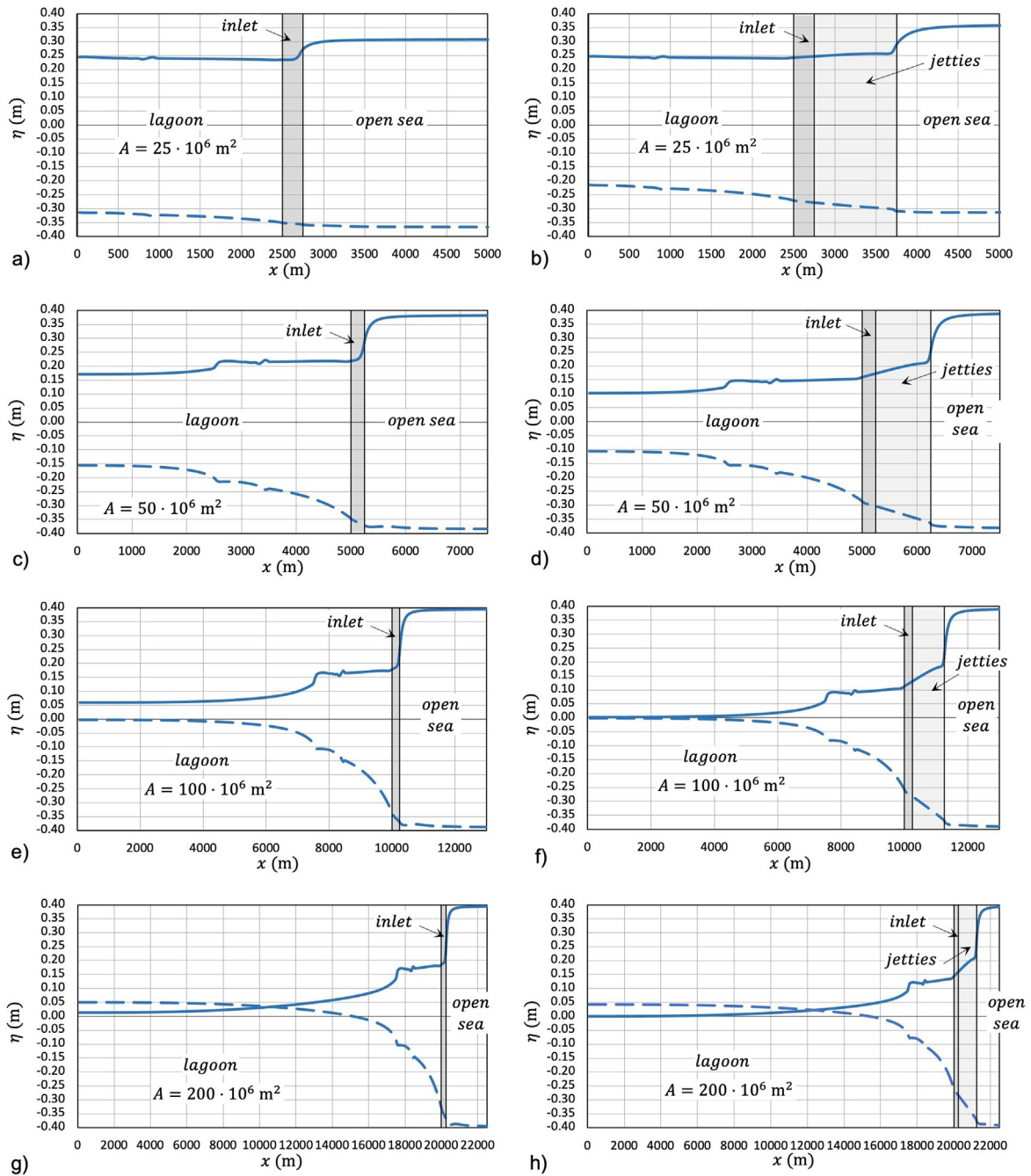


FIG. 11. Tide profiles obtained with the 2DH model, along a longitudinal section of the inlet, in the instants of maximum tidal gradient during both flood (solid line) and ebb (dashed line) phases, for surface basins equal to (a) $A = 25 \cdot 10^6 \text{ m}^2$ without jetties, (b) $A = 25 \cdot 10^6 \text{ m}^2$ with jetties, (c) $A = 50 \cdot 10^6 \text{ m}^2$ without jetties, (d) $A = 50 \cdot 10^6 \text{ m}^2$ with jetties, (e) $A = 100 \cdot 10^6 \text{ m}^2$ without jetties, (f) $A = 100 \cdot 10^6 \text{ m}^2$ with jetties, (g) $A = 200 \cdot 10^6 \text{ m}^2$ without jetties, and (h) $A = 200 \cdot 10^6 \text{ m}^2$ with jetties.

tides was 1.1 m in Grado and Trieste, and 1.05 m in Venice Lido and the Venice oceanographic tower.

The hydrological surface A is a very delicate parameter to estimate the tidal prism, and when referring to past data, it is necessary to

take into account the variations in mean sea levels due to climate change. In the northern Adriatic, from 1950 to today, the mean sea level has increased by +0.13 m. To estimate the current hydrological surface area A of the Lignano, Buso, and Grado basins, the effects of

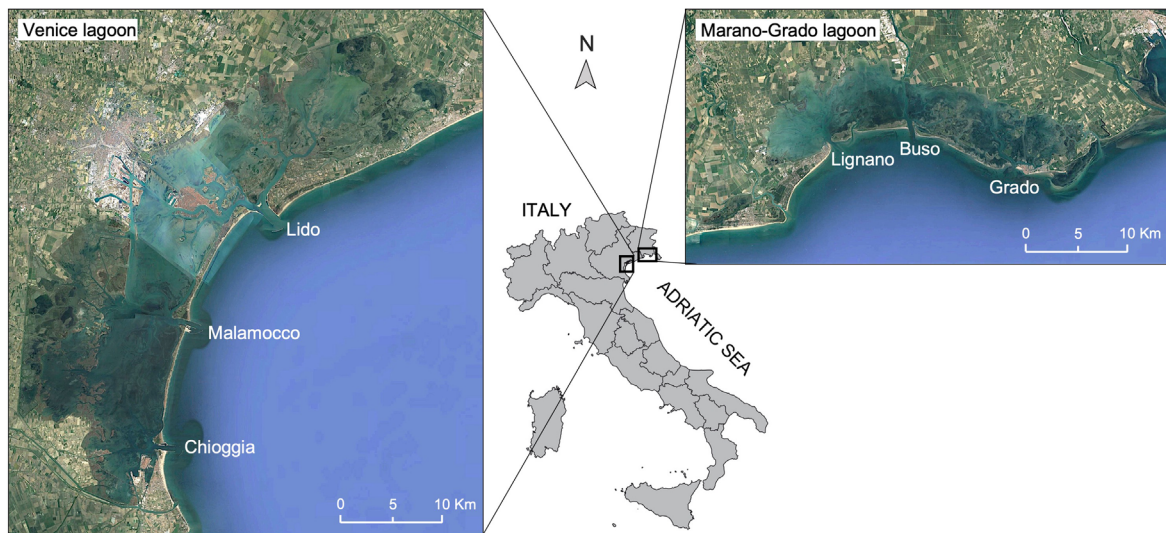


FIG. 12. Venice and Marano-Grado lagoons.

climate changes and anthropic interventions were taken into account. In particular, this was done while considering the surface increases due to the mean sea level rise, but also the losses due to the construction of fishing valleys and artificial islands used in the past for the relocation of dredging material within the lagoon. These evaluations were done in comparison to the Dorigo map (1965).

To verify relationships (46) and (37), the most significant basins were considered, namely, Lignano, Buso, and Grado for the Marano-Grado lagoon and Lido, Malamocco, and Chioggia for the Venice lagoon. For each basin, reference was made to experimental prism measurements (Dorigo, 1965; CVN, 1989) and to prisms estimated with simulations made using the 2DH model mentioned above.

Table V shows the geometric characteristics of the considered basins, i.e., the presence/absence of jetties, the hydrological surface A , the minimum flow cross-sectional area below mean sea level Ω , the tidal prism P , and the tidal amplitude a_m , together with information concerning measured or simulated prisms and reference year. In 2DH simulations, a sinusoidal tide of amplitude a_m and period $T = 12$ h was

used. These values are derived from a zero-crossing analysis of tide gauges measurements carried out in the Marano and Grado lagoon (Petti *et al.*, 2018), and they correspond to the average spring tidal characteristics in the northern Adriatic Sea, as also reported by Dorigo (1965).

Table VI shows, for each inlet, the measured (or simulated) prisms and the estimated prisms with the relationships (46) and (37).

The quantities B and L represent the average width and length of the inlet channel, respectively. For the estimation of the γ parameter [Eq. (12)], a rectangular cross-section with average depth $h = \Omega/B$ was considered for each channel. The shape of the section is generally unknown, and in order to ensure the ease of use of relations (37) and (46), we believe that the approximation to the rectangular section is the optimal choice, since the width of lagoon inlets is at least an order of magnitude greater than the water depth. Furthermore, to each channel, a coefficient $k_s = 30 \text{ m}^{1/3} \text{ s}^{-1}$ was assigned, which is representative of a movable bed characterized by the presence of dunes having an average height of 0.40 m and a length of about 4 m (Van Rijn,

TABLE V. Geometric characteristics and tidal prisms (measured or simulated) of some basins in the Marano-Grado and Venice lagoons.

Prism	Inlet	Jetties	Lagoon	$A \text{ (m}^2 \cdot 10^6\text{)}$	$\Omega \text{ (m}^2\text{)}$	$P \text{ (m}^3 \cdot 10^6\text{)}$	$a_m \text{ (m)}$	Date of survey
Measured	Lignano	No	Marano	42.5	3900	48.14	0.52	1961 (Dorigo, 1965)
	Buso	No	Grado	29	2216	27.20	0.56	1950 (Dorigo, 1965)
	Grado	No	Grado	22.5	1970	21.25	0.50	1950 (Dorigo, 1965)
	Lido	Two	Venezia	155	7916	145	0.50	1984 (CVN, 1989)
	Malamocco	Two	Venezia	130	7320	136	0.50	1984 (CVN 1989)
	Chioggia	Two	Venezia	82	4840	82	0.50	1984 (CVN, 1989)
Simulated	Lignano	No	Marano	43	2600	43.45	0.55	2021
	Buso	Two	Grado	30	2750	30.40	0.55	2021
	Grado	Two	Grado	24.0	2000	24.72	0.55	2021

TABLE VI. Comparison of measured (or simulated) and estimated tidal prisms in some basins in the Marano-Grado and Venice lagoons. $P^{(H)}$ has been evaluated by means of Eq. (46) and ζ has been deduced from the curves in Fig. 10. B and L , for simulated data, have been taken from satellite pictures, measured data refer to the survey specified in Table V.

Prism	Inlet	B (m)	L (m)	λ	γa_m	ζ ($\text{m}^3 \cdot 10^6$)	E_m ($\text{m}^3 \cdot 10^6$)	P	$P^{(H)}$	$\varepsilon_p\%$
Measured	Lignano	670	400	0.60	24.59	1.62	0.23	48.14	44.32	7.94
	Buso	340	300	0.93	40.73	1.77	0.34	27.20	32.27	18.64
	Grado	400	350	0.67	28.88	1.60	0.24	21.25	22.52	5.98
	Lido	900	2100	1.07	14.35	2.57	1.24	145	139.44	3.83
	Malamocco	500	2000	0.73	10.60	2.46	0.80	136	128.88	5.24
	Chioggia	570	2000	0.86	12.78	2.42	0.91	82	79.00	3.66
Simulated	Lignano	340	400	1.21	40.63	1.96	0.57	43.45	46.04	5.96
	Buso	440	1700	0.57	11.42	2.13	0.44	30.47	33.44	9.75
	Grado	400	350	0.93	38.86	2.20	0.35	24.72	26.23	6.11

1984), as detected at the Lignano inlet. We assumed that these features are also present in the other inlets analyzed, as they are similar both in the sediment size (OGS, 2004) and in the current maximum velocities. Furthermore, this coefficient is consistent with the data reported by Tambroni and Seminara (2006) on the inlets of the Venice lagoon.

As can be seen (Table VI), all errors $\varepsilon_p\%$ are less than 10%, except for the prism measured and estimated in the Buso basin in 1950. It is difficult to justify this result since this basin does not present substantial differences compared to the others, so there may have been a measurement error.

Since 1950, this basin has undergone some important changes as a result of anthropic interventions; in particular, two jetties were built with the aim to protect the inlet, and the channel was deepened in order to guarantee the access of boats to a commercial port located within the lagoon. The presence of jetties generally involves a reduction in the prism, due to the increase in energy losses both before the entrance (greater ζ value) and distributed along the channel; on the contrary, the deepening of the channel favors a greater flow and consequently a higher prism. The response of the lagoon inlet-basin system determined in this study is able to provide an estimate on the variation of the prism due to a change in one of the parameters on which it depends, at least in a transition phase that does not involve significant changes to other quantities. In this sense, Eqs. (37) and (46) are also suitable for studying the effects on the prism value due to an anthropic intervention. For example, even the Lignano inlet has undergone a narrowing trend in recent decades, after the construction of the pier to protect the port located close to the inlet itself. The effects of this narrowing on the prism have been numerically analyzed in Petti *et al.* (2021), and, in particular, they can be examined through the simple relations proposed in this work, as done in the case above.

These considerations also underline that Eqs. (37) and (46) are easy to apply in real contexts, provided that all the required geometric and hydrodynamic parameters are available and correctly defined.

B. Fire Island Inlet

As a second check of relationships (46) and (37), it was decided to apply them to the basin of the Fire Island Inlet, in the United States.

Fire Island Inlet is one of six permanent inlets located on the south coast of Long Island, New York, and connects the Great South

Bay to the Atlantic Ocean (Fig. 13). Bonisteel *et al.* (2004) reported that the inlet has a depth of about 3.7 to 4.3 m at mean sea level, a width of approximately 1070 m, and a length from the barrier of about 5650 m. The total length of the inlet extends for 6500 m from the entrance to Great South Bay (Kraus *et al.*, 2003), and the basin connected to the inlet has a geographical area of about $270 \cdot 10^6 \text{ m}^3$.

Long Island and the associated inlets have been studied by numerous researchers, both for problems related to navigation and solid transport (e.g., Saville, 1960; Panuzio, 1968; Morang *et al.*, 1999; and Kumar and Saunders, 1974), and for hydrodynamic aspects related to the estimation of the tidal prism (O'Brien, 1931; Jarrett, 1976).

From the hydrodynamic point of view, one of the reasons why this site was particularly interesting is the large number of tide gauges located in the basin. Jarrett (1976) conducted a very thorough investigation of the tidal prism flowing through the Fire Island Inlet, and using the cubature method, he found the value $P = 52.67 \cdot 10^6 \text{ m}^3$. Jarrett showed both the planimetry, depicted here on a recent satellite image (Fig. 13), and the tidal measurements, summarized in Table VII, used for the estimation of the prism in his work.

It is thanks to the quantity of data available, not easily findable in other sites, that it was decided to verify the relationships (46) and (37) in this basin.

Jarrett, in addition to the estimate of the prism, also provides the minimum flow cross-sectional area below the mean sea level, equal to 3725 m^2 , and the average water depth in the inlet $h = 4.5 \text{ m}$ in his work. To use relationships (46) and (37), we need the average section of the inlet Ω , greater than the minimum flow cross-sectional area; for this reason, Ω has been estimated assuming a simple rectangular shape. The value found by Jarrett was maintained as the average depth h of the inlet, and the value $B = 1070 \text{ m}$ was assumed as the average width, both are consistent with the values found by Bonisteel *et al.* (2004) and, as regards B , with the map shown in Fig. 13. $L = 6500 \text{ m}$ was assumed as the length of the inlet, a value provided by Kraus *et al.* (2003) and consistent with the plan shown in Fig. 13.

For the hydrological area of the basin, with the help of the map shown in Jarrett (1976), the value $A = 250 \cdot 10^6 \text{ m}^2$ was estimated, while for the tidal range in ocean through the values reported in Table VII, we have deduced the value $2a_m = 1.25 \text{ m}$. From the same table, we also deduced the tidal range within the basin, which results as



FIG. 13. Fire Island Inlet and Great South Bay (New York)—location of tidal stations, as shown by Jarrett (1976).

TABLE VII. Values of maximum (η_{max}), minimum (η_{min}), and correspondent excursion ($2a_l$) of tidal levels, deduced from measurements in the Fire Island Inlet and Great South Bay (New York), as shown in Jarrett (1976). The stations are located as depicted in Fig. 13.

Station	η_{max} (m)	η_{min} (m)	$2a_l$ (m)
Ocean	0.63	-0.63	1.26
STA 62	0.12	-0.13	0.25
STA 63	0.11	-0.12	0.24
STA 64	0.11	-0.10	0.22
STA 65A	0.11	-0.11	0.23
STA 66	0.11	-0.12	0.24
STA 68	0.11	-0.11	0.22
STA 69A	0.30	-0.29	0.59
STA 70	0.40	-0.40	0.80

TABLE VIII. Geometric characteristics and tidal prism estimated by Jarrett in Fire Island Inlet-Great South Bay (O'Brien, 1931; Kraus et al., 2003; and Bonisteel et al., 2004).

A ($m^2 \cdot 10^6$)	B (m)	h (m)	L (m)	P ($m^3 \cdot 10^6$)	$2a_m$ (m)	$2a_l$ (m)
250	1070	4.5	6500	52.67	1.25	0.23

TABLE IX. Comparison of measured and estimated tidal levels and prisms in Fire Island Inlet-Great South Bay.

k_s ($m^{1/3} s^{-1}$)	γa_m	λ	ξ	E_m	$2a_l$ (m)	$2a_l^{(H)}$ (m)	P ($m^3 \cdot 10^6$)	$P^{(H)}$ ($m^3 \cdot 10^6$)	ϵ_{a_l} %	ϵ_P %
30	57.51	12.27	2.76	41.87	0.23	0.22	52.67	55.60	4.35	5.56

$2a_l = 0.23$ m. Table VIII shows a summary of the geometric characteristics and tidal prism estimated by Jarrett in Fire Island Inlet-Great South Bay.

To apply the relationships (46) and (37), we need the coefficients k_s and ξ . Based on a morphological analogy, i.e., the same sandy grain size and maximum velocity (Wolff, 1975; OGS, 2004), for the former, the value $k_s = 30 m^{1/3} s^{-1}$ was assumed, the latter was estimated using the curves shown in Fig. 10. Table IX shows the results obtained by applying the relationships (46) and (37), including the mean tidal range inside the basin $2a_l^{(H)} = 2a_m H$. As can be seen, the estimation error is in line with those obtained for the Italian lagoons.

The greater value of the prism $P^{(H)}$ compared to P can be attributed, only for a small part, to the shape of the inlet section assumed to be rectangular.

VI. DISCUSSION AND CONCLUSIONS

A correct estimate of the tidal prism is very important as several factors, both environmental and more specifically hydro-morphodynamic, depend on its value. However, as widely discussed, relationships (1) and (2) used to date show a wide range of uncertainty depending on the parameters and coefficients chosen. The approach used in this paper is dynamic and simultaneously involves several hydrodynamic and geometric factors that describe the entire “lagoon inlet-basin” system. The prism is the hydrodynamic response of this system, seen as a nonlinear damped harmonic oscillator forced by the tidal level fluctuation on the sea side. Its approximate solution, with a relative small margin of error, is represented by the relationships (46)

and (37), through which it is possible to estimate the tidal prism in a relatively simple way. This is an important result because it summarizes the various empirical approaches developed, without losing their practicality, in particular in the design field. At the same time, by applying an analytical treatment, the proposed approach is able to rigorously interpret the hydrodynamic behavior of a tidal inlet as a function of its main parameters. Several interesting aspects from the scientific point of view have been emerged and are discussed below, concerning, in particular, the nonlinearity of the system, the possible resonance phenomenon, the channeling effect, and the comparisons with experimental and numerical data.

The prism has often been considered as an almost constant quantity for an assigned basin and tidal inlet, and it has been measured or estimated in different ways. However, as shown, it depends on the basin extension A , the cross section Ω , the length L , and the roughness coefficient k , (or equivalent) of the inlet; on the head loss coefficient ζ ; on the tidal amplitude a_m and period T ; and on the presence or absence of jetties. With relationships (46) and (37), though only approximately, it is possible to take into account all these quantities with the advantage of being able to make predictions in the case, for example, of human interventions on the inlet. This can be very useful thinking of a stabilization through the jetties or a modification of the inlet geometry, which can lead, for example, to a narrowing, as in the case of Lignano discussed earlier.

In this regard, the pioneering work of Mehta and Özsoy (1978), who determined the response of the lagoon inlet-basin system considering most of these variables, should be considered. The response expressed in the form given by Eq. (39), as a function of the dimensionless variables of the present study, provides the possibility to determine the tidal prism in a more complete way than Eqs. (1) and (2), even if the dissipative term of the 1D momentum equation has been linearized. However, the present model has the advantage of further simplifying the Mehta and Özsoy expression, globally reducing the error in the estimation of the tidal prism as a function of the dimensionless variable γa_m , as can be seen from Fig. 8(b).

More recently, Larson *et al.* (2020) proposed a semi-analytical approach to describe the main hydrodynamic properties of the flow exchanged between the sea and a lagoon system. The authors recognize the importance of deriving simple expressions between the main tidal inlet hydrodynamic variables, which although not exact, satisfy the governing equations in a general sense according to a specified criterion. This is an academic topic still open with important aspects from both a scientific and a practical point of view. The relationships proposed by Larson *et al.* are also expressed in a dimensionless form, but are applicable only in contexts where the conditions (29) can be satisfied. Larson *et al.* started from a simplified form of Eq. (3) where the inertial term is neglected. Furthermore, the terms related to the channeling process, i.e., the transformation of potential energy into the kinetics and the bottom frictional losses before the inlet entrance, which have significant weight, were not taken into account. Similarly, Mehta and Özsoy (1978) did not consider the channeling process.

In fact, another aspect this work has focused on is the head loss coefficient $\zeta = \zeta_{en} + \zeta_{ex} + \zeta_{eq}$. In the literature, reference is often made to works that have hydraulic analogies with inlets, such as turbulent jets, and Bruun (1978) mentions them citing the works of Daily and Harleman (1966) and Dean (1971). On the basis of the results provided by these authors, Bruun suggests assuming

$\zeta_{en} + \zeta_{ex} = 1.05 - 1.25$, even though he evaluates the work of Mei *et al.* (1974) as interesting, who study the separation losses due to a narrow constriction under oscillatory flow field analytically. Based on these results, Bruun concludes that $\zeta_{en} + \zeta_{ex}$ can reach a maximum value close to 2.8.

In this paper, a new coefficient ζ_{eq} was introduced to take into account the head losses at the bottom in the flow channeling path before the inlet, both in the ebb and flow phase. Using simplified schemes of lagoon basins and a 2DH numerical model, we have provided a first experimental estimate of the overall coefficient $\zeta = \zeta_{en} + \zeta_{ex} + \zeta_{eq}$, finding that this depends on the surface of the basin A , on the tide ωa_m and on the inlet section Ω (Fig. 10). These parameters are likely to affect ζ_{eq} more than $\zeta_{en} + \zeta_{ex}$. In fact, the values of ζ found in this first approach are included in the range 1.5–3.5 to which the contribution of the kinetic energy should also be added. These values are consistent with the studies by Mei *et al.* (1974), thus confirming the need to consider the distributed energy loss component in the current channeling phase before the inlet.

Furthermore, through the coefficient ζ , we have also tried to quantify the influence of the jetties on the estimate of the tidal prism in this work, a problem highlighted several times by many authors and often solved by grouping the inlets by classes (O'Brien, 1931; 1969; Jarrett, 1976). The problem was always addressed numerically using the simplified schemes of the previous lagoon basins and adding 1000 m long jetties to the inlet. The results depicted in Fig. 10 show an average increase in ζ of 25% compared to identical configurations without jetties. In this case, given the sharp corners introduced by the jetties, it is believed that the increase in ζ is due more to a growth of $\zeta_{en} + \zeta_{ex}$ than of ζ_{eq} .

The new relationships (46) and (37) differ from (1) also because the assumption of an equilibrium condition is not considered, but they can be applied in any context, once all the geometric and hydrodynamic characteristics are assigned. This guarantees and confirms the greater generality and applicability of these relationships and also opens up the search for a new condition of morphological equilibrium of the tidal inlets.

For the estimation of the equilibrium minimum flow cross section in many works (e.g., O'Brien, 1931; 1969; Jarrett, 1976; Powell *et al.*, 2006; and Fontolan *et al.*, 2007), reference is made to the morphological relationship (1), where the tidal prism is estimated either with the cubature method or with the current data method (Jarrett, 1976), very often simply Eq. (2) is used considering the offshore tidal range. Obviously, if the goal is to find the minimum equilibrium section, the tidal prism is assumed to be constant.

Actually, as has emerged from the present work, this is not the case. In fact, using the hydrodynamic relationship (45), the results shown in Fig. 5 and re-adapting the morphological relationship (1), we can plot the curves shown in Fig. 14.

Two important results achieved with the present work and summarized in Fig. 5 are (a) the tidal prism is not constant but depends on the main characteristics of both the inlet section and the basin as well as the tide; all these factors are summarized in the dimensionless variable $\sqrt{\Omega g / (AL\omega^2)}$; (b) the area of the equilibrium section is determined not only by the condition of dynamic equilibrium linked to the sediment transport but also by the condition of equilibrium between the tidal prism and the morphological relationship. As $\sqrt{\Omega g / (AL\omega^2)}$ increases, the prism tends toward the asymptotic value P_0 and the

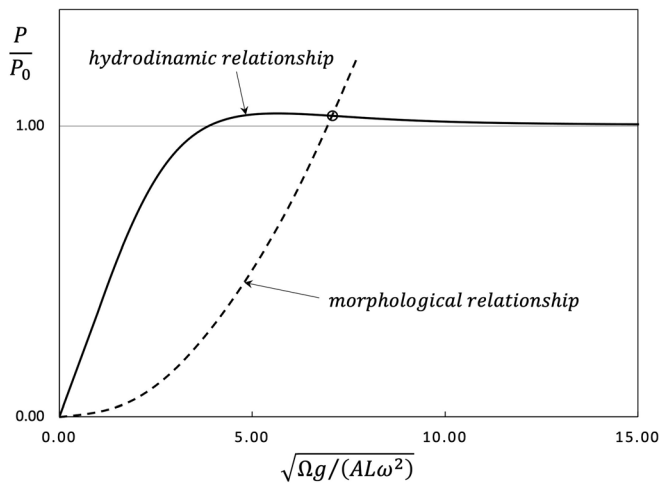


FIG. 14. Tidal prism: example of trend of dimensionless hydrodynamic [Eq. (45)], for an assigned γ_{am} value, and morphological [Eq. (1)] relationships vs $\sqrt{\Omega g/(AL\omega^2)}$. It should be observed that the hydrodynamic curve changes with the variation of γ_{am} (5), while the morphological one changes with the variation of k and α [Eq. (1)].

value of this variable beyond which $P = P_0$ depends on γ_{am} . When $\gamma_{am} \lesssim 40$ and $\sqrt{\Omega g/(AL\omega^2)} \lesssim 10$ (Fig. 5), a resonance phenomenon may occur, and the tidal amplitude inside the lagoon may be greater than outside, with a prism also greater than $2a_m A$. However, this phenomenon is more likely to occur in a small basin, such as a harbor basin, than in a normal lagoon basin.

The use of dimensionless variables has made it possible not only to avoid transition problems between different measurement systems but also to better highlight the interdependence of the prism on the various factors taken into consideration. In particular, ω/ω_N compares the tidal frequency to the lagoon oscillation mode, while γ_{am} summarizes all the distributed and concentrated energy losses, both not only across the inlet but also in a much larger proximal area due to the channeling current effect that has been taken into consideration for the first time in the present approach.

Another aspect to underline concerns the nonlinearity parameter. The basins tested showed different degrees of nonlinearity: weak for those of the northern Adriatic ($E_m \leq 1.24$) and strong for the Atlantic one of the Fire Islands ($E_m = 41.87$); however, in all cases, the error estimate of the prism was less than 10%. The only exception is the measured prism of the Buso basin, where, however, it is believed that a measurement or transcription error may be possible. On the other hand, what is observed is that as the nonlinearity parameter E_m increases, the tidal prism decreases, sometimes even significantly, as in the case of the Fire Islands.

The last important consideration is that the results obtained in this work are based on the assumption of a constant mean cross-sectional flow area below the mean sea level. This means that a constant still water depth and inlet channel width are assumed. For this reason, the present model cannot reproduce the hydrodynamic effects of a mean sea level varying in time during the tidal cycle, as happens, for example, in the fortnightly tides that occur in a choked lagoon (e.g., Hill, 1994; MacMahan et al., 2014; de Brito Jr. et al., 2018). On

the other hand, it is possible to take into account the effects on the prism of a static mean sea level rise, due, for example, to climate changes, by reconsidering correct values of the depth and width of the tidal inlet and of the lagoon hydrological surface.

In conclusion, by means of a 1D dynamic approach, based on the harmonic response of a nonlinear system, the study of the hydrodynamic estimation of the tidal prism was addressed. The following main conclusions can be drawn from this study:

- (1) The tidal prism is not constant but depends not only on the tide but also on the main geometric and dynamic characteristics of both the inlet and the lagoon basin, through the dimensionless variables γ_{am} and $\sqrt{\Omega g/(AL\omega^2)}$.
- (2) To estimate the tidal prism, a relatively simple hydrodynamic relationship has been determined, a relationship that requires only the calibration of a coefficient ξ , carried out here using 2DH numerical simulations performed on simplified basins.
- (3) It has been verified on real cases that the relationship found provides an estimate of the prisms with an error of less than 10%, both for linear and highly nonlinear basins.

In future work, a more in-depth investigation for the estimation of ξ is needed, both numerical and experimental, with and without jet-ties, and by varying other geometric parameters of the tidal inlet or for different values of the Gauckler–Strickler coefficient in the domain, taking into account bed morphologies, which could interact with the tidal currents, increasing flow resistance (Dey et al., 2020; Mercier and Guillou, 2021). Furthermore, it would be useful to expand the verifications of the proposed relationship on other instrumented basins.

AUTHOR DECLARATIONS

Conflict of Interest

The authors have no conflicts to disclose.

Author Contributions

Marco Petti: Conceptualization (equal); Data curation (equal); Formal analysis (equal); Investigation (equal); Methodology (equal); Resources (equal); Software (equal); Supervision (equal); Validation (equal); Visualization (equal); Writing – original draft (equal); Writing – review & editing (equal). **Sara Pascolo:** Conceptualization (equal); Data curation (equal); Formal analysis (equal); Investigation (equal); Methodology (equal); Resources (equal); Software (equal); Supervision (equal); Validation (equal); Visualization (equal); Writing – original draft (equal); Writing – review & editing (equal). **Silvia Bosa:** Conceptualization (equal); Data curation (equal); Formal analysis (equal); Investigation (equal); Methodology (equal); Resources (equal); Software (equal); Supervision (equal); Validation (equal); Visualization (equal); Writing – original draft (equal); Writing – review & editing (equal). **Nadia Busetto:** Conceptualization (equal); Data curation (equal); Formal analysis (equal); Investigation (equal); Methodology (equal); Resources (equal); Software (equal); Supervision (equal); Validation (equal); Visualization (equal); Writing – original draft (equal); Writing – review & editing (equal).

DATA AVAILABILITY

The data that support the findings of this study are available from the corresponding author upon reasonable request.

APPENDIX: STRONGLY AND WEAKLY DAMPED HARMONIC OSCILLATORS

If $\lambda > 1$, the solution to the system (34), called strongly damped, is

$$\bar{\eta}^* = \left[a_{s1}^* e^{-\frac{\omega_N}{\omega}(\lambda - \sqrt{\lambda^2 - 1})t^*} + a_{s2}^* e^{-\frac{\omega_N}{\omega}(\lambda + \sqrt{\lambda^2 - 1})t^*} \right] + H_I \sin[t^* - (\tau^* + \phi_I)]. \tag{A1}$$

If $\lambda = 1$, the solution of the system, called critical damping, is

$$\bar{\eta}^* = \left[a_{s1}^* e^{-\frac{\omega_N}{\omega}t^*} + a_{s2}^* t^* e^{-\frac{\omega_N}{\omega}t^*} \right] + H_I \sin[t^* - (\tau^* + \phi_I)]. \tag{A2}$$

If $\lambda < 1$, the solution of the system, called weakly damped, is

$$\bar{\eta}^* = a_s^* e^{-\lambda \frac{\omega_N}{\omega} t^*} \cos \left[\sqrt{1 - \lambda^2} \left(\frac{\omega_N}{\omega} \right) t^* + \psi \right] + H_I \sin[t^* - (\tau^* + \phi_I)]. \tag{A3}$$

a_{s1}^* , a_{s2}^* , a_s^* , and ψ are constants that depend on the initial conditions, while

$$H_I(\gamma a_m, \omega/\omega_N) = \frac{1}{\sqrt{\left[1 - \left(\frac{\omega}{\omega_N} \right)^2 \right]^2 + \left[\frac{\gamma a_m}{2} \left(\frac{\omega}{\omega_N} \right)^2 \right]^2}} \tag{A4}$$

and

$$\phi_I(\gamma a_m, \omega/\omega_N) = \tan^{-1} \left[\frac{\frac{\gamma a_m}{2} \left(\frac{\omega}{\omega_N} \right)^2}{1 - \left(\frac{\omega}{\omega_N} \right)^2} \right]. \tag{A5}$$

The quantities $H_I(\gamma a_m, \omega/\omega_N)$ and $\phi_I(\gamma a_m, \omega/\omega_N)$ provide the amplitude response [Fig. 15(a)] and the phase lag [Fig. 15(b)] of the linear system (34).

Returning to the system (34), in all cases, as t^* approaches ∞ , the solution tends to $H_I \sin(t^* - \theta)$. Particularly, in the case $\lambda > 1$, after a time $t_e^* \cong 5\theta$, named exhaustion time, with $\theta = (\omega/\omega_N)/(\lambda - \sqrt{\lambda^2 - 1})$, the first term of (A1), that is the damped aperiodic

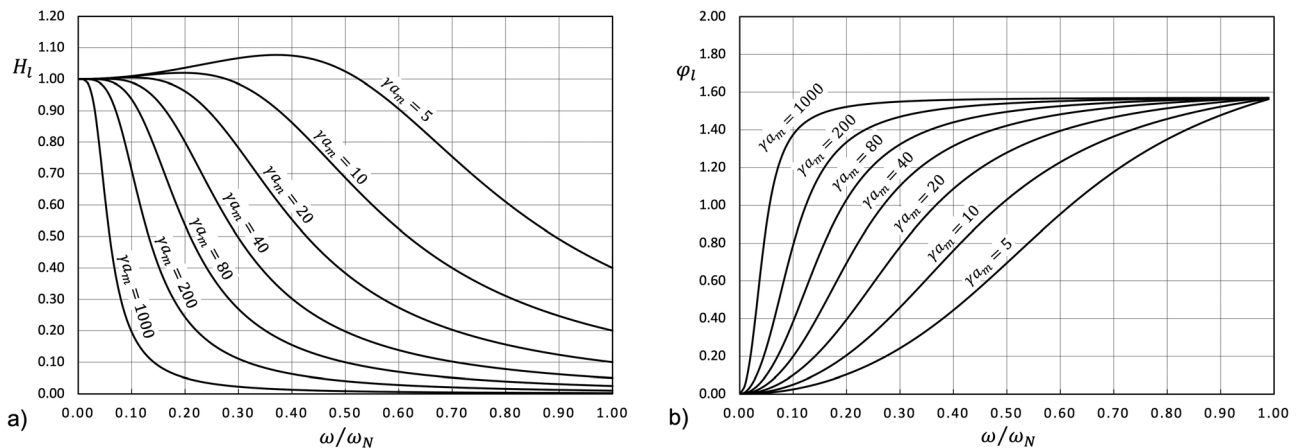


FIG. 15. Linear system (34): (a) amplitude response for values $\gamma a_m = [5, 1000]$ and (b) phase lag response for values $\gamma a_m = [5, 1000]$ and $\tau^* = 0$.

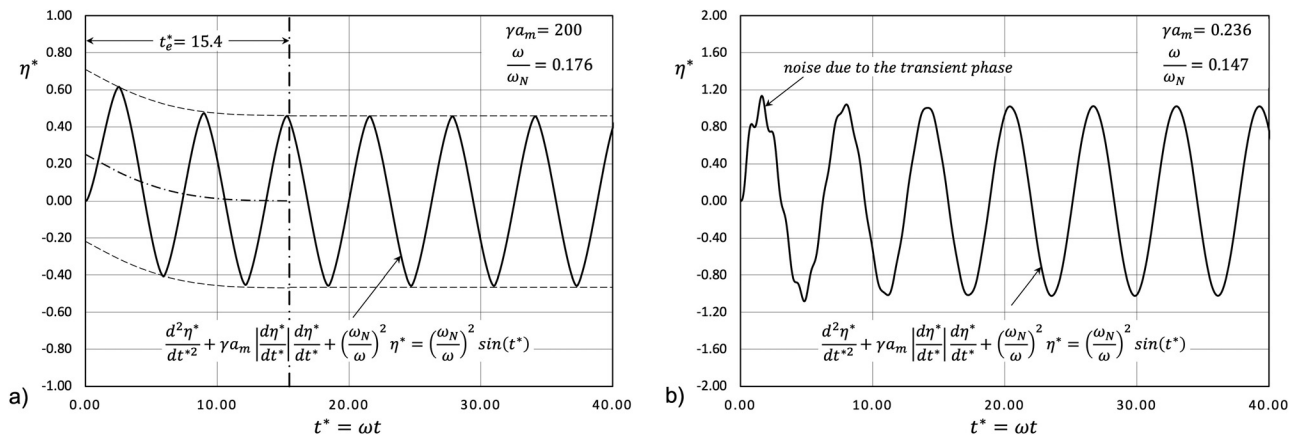


FIG. 16. Example of transients: (a) in a strongly damped lagoon system ($t_e^* = 15.4$; $E_m = 6.20$) and (b) in a slightly damped lagoon system ($t_e^* = 84.7$; $E_m = 5.1 \cdot 10^{-3}$).

motion in square brackets, is reduced to less than 1%. As an example, Fig. 16(a) shows the dimensionless numerical solution of a strongly damped system, obtained by integrating the differential Eq. (27) with a second order finite difference numerical method.

In the case $\lambda < 1$, the transient phase, first term to the right of Eq. (A3), appears in the form of a disturbance at the first oscillations induced by the forcing $H_I \sin(t^* - \phi_I)$; the transient ends when $t_e^* \cong 5\theta$, with $\theta = \omega/\omega_N/\lambda$. As an example, Fig. 16(b) shows the dimensionless numerical solution of a slightly damped system, obtained by integrating the differential equation (27) with the same second order finite difference numerical method.

In both cases, if $t^* > t_e^*$, the solution of the system (34) is

$$\bar{\eta}^* \cong H_I \sin(t^* - \theta), \quad (\text{A6})$$

where

$$\theta = \phi_I + \tau^* \quad (\text{A7})$$

and H_I and ϕ_I are given by Eqs. (A4) and (A5). It is interesting to observe how the linear response of a lagoon system, Eq. (A4), differs from that of a viscous mechanical system for the term $(\omega/\omega_N)^4$ instead of $(\omega/\omega_N)^2$ in the amplitude response and $(\omega/\omega_N)^2$ instead of (ω/ω_N) in the phase lag response (A5).

The exhaustion time t_e^* plays an important role when we want to study a lagoon system through any numerical approach. In fact, while in reality, the transient does not exist because the tidal oscillation persists continuously, a numerical simulation often starts from a flat sea state. In this case, it is necessary to pay close attention to the solution obtained in the interval of time $t^* < t_e^*$ because it is not realistic.

REFERENCES

- Bonisteel, J. M., Peters-Snyder, M., and Zarillo, G. A., "Barrier island migration and morphologic evolution, Fire Island Inlet, New York," *J. Am. Shore Beach Preserv. Assoc.* **72**, 21–24 (2004).
- Bruun, P., *Stability of Tidal Inlets: Theory and Engineering* (Elsevier Scientific Publishing, Amsterdam, 1978).
- CVN, *Consorzio Venezia Nuova - Progetto Preliminare di Massima Delle Opere Alle bocche - Descrizione Dell'ecosistema, Parte II* (Ministero dei Lavori Pubblici, Magistrato alle Acque di Venezia, Venezia, 1989), Vol. 2 (in Italian).
- Daily, J. W. and Harleman, D. R. F., *Fluid Dynamics* (Addison Wesley Publishing Company, Reading, MA, 1966).
- D'Alpaos, A., Lanzoni, S., Marani, M., and Rinaldo, A., "On the tidal prism-channel area relations," *J. Geophys. Res.* **115**, F01003, <https://doi.org/10.1029/2008JF001243> (2010).
- de Brito, A. N., Jr., Fragoso, C. R., Jr., and Larson, M., "Tidal exchange in a choked coastal lagoon: A study of Mundaú Lagoon in northeastern Brazil," *Reg. Stud. Mar. Sci.* **17**, 133–142 (2018).
- De Falco, M. C., Adduce, C., Cuthbertson, A., Negretti, M. E., Laanearu, J., Malcangio, D., and Sommeria, J., "Experimental study of uni- and bi-directional exchange flows in a large-scale rotating trapezoidal channel," *Phys. Fluids* **33**, 036602 (2021).
- Dean, R. G., *Hydraulics of Inlets* (Department of Coastal and Oceanographic Engineering, University of Florida, Gainesville, 1971).
- Dey, S., Paul, P., Fang, H., and Padhi, E., "Hydrodynamics of flow over two-dimensional dunes," *Phys. Fluids* **32**, 025106 (2020).
- Dey, S., Rathore, V., Penna, N., and Gaudio, R., "Hydrodynamics of flow over a gradually varied bed roughness," *Phys. Fluids* **33**, 125112 (2021).
- Dorigo, L., *La Laguna di Grado e le Sue Foci - Ricerche e Rilievi Idrografici* (Magistrato Alle Acque, Ufficio Idrografico, Venice, Italy, 1965) (in Italian).
- Engelund, F. and Hansen, E., *A Monograph on Sediment Transport* (Technisk Forlag, Copenhagen, 1967).
- Escoffier, F. F., "The stability of tidal inlets," *Shore Beach* **8**(4), 111–114 (1940).
- Escoffier, F. F., *Hydraulics and Stability of Tidal Inlets* (Coastal Engineering Research Center, US Army Corps of Engineers, Fort Belvoir, VA, 1977).
- Fontolan, G., Pillon, S., Delli Quadri, F., and Bezzi, A., "Sediment storage at tidal inlets in northern Adriatic lagoons: Ebb-tidal delta morphodynamics, conservation and sand use strategies," *Estuarine, Coastal Shelf Sci.* **75**, 261–277 (2007).
- Gao, S. and Collins, M., "Tidal inlet stability in response to hydrodynamic and sediment dynamic conditions," *Coastal Eng.* **23**, 61–80 (1994).
- Helsby, R., Amos, C. L., and Umgieser, G., *Tidal Prism Variation and Associated Channel Stability in N. Venice Lagoon* (Scientific Research and Safeguarding of Venice, Multigraf, Spinea, 2008), Vol. VI.
- Hill, A. E., "Fortnightly tides in a lagoon with variable choking," *Estuarine, Coastal Shelf Sci.* **38**, 423–434 (1994).
- Hughes, S. A., "Equilibrium cross-sectional area at tidal inlets," *J. Coastal Res.* **18**, 160–174 (2002).
- Jarrett, J. T., *Tidal Prism-Inlet Area Relationships* (Coastal Engineering Research Center, US Army Corps of Engineers, Fort Belvoir, VA, 1976).
- Keulegan, G. H., "Tidal flow in entrances water-level fluctuations of basins in communication with seas," Technical Bulletin No. 14 (Committee on Tidal Hydraulics, U.S. Army Station, Vicksburg, MS, 1967).
- Kraus, N. C., Zarillo, G. A., and Tavolaro, J. F., "Hypothetical relocation of Fire Island Inlet, New York," in *Proceedings of Coastal Sediments '03 (CD-ROM)* (World Scientific Publishing Corp., 2003).
- Krishnamurthy, M., "Tidal prism of equilibrium inlets," *J. Waterway, Port, Coastal, Ocean Div.* **103**(4), 423–432 (1977).
- Kumar, N. and Saunders, J. E., "Inlet sequence: A vertical succession of sedimentary structures and textures created by the lateral migration of tidal inlets," *Sedimentology* **21**, 491–532 (1974).
- Larson, M., Nunes, A., and Tanaka, H., "Semi-analytic model tidal-induced inlet flow morphological evolution," *Coastal Eng.* **155**, 103581 (2020).
- LeConte, L. J., "Discussion on the paper, 'Notes on the improvement of river and harbor outlets in the United States' by D. A. Watt," *Trans. ASCE* **55**, 306–308 (1905).
- MacMahan, J., van de Kreeke, J., Reniers, A., Elgar, S., Raubenheimer, B., Thornton, E., Weltmer, M., Rynne, P., and Brown, J., "Fortnightly tides and subtidal motions in a choked inlet," *Estuarine, Coastal Shelf Sci.* **150**, 325–331 (2014).
- Marchi, E., "Sulla stabilità delle bocche lagunari a marea," *Rend. Lincei* **1**, 137–150 (1990) (in Italian).
- Mehta, A. J. and Özsoy, E., "Flow dynamics and nearshore transport," in *Stability of Tidal Inlets*, edited by P. Bruun (Elsevier Scientific Publishing Company, Amsterdam, 1978).
- Mei, C. C., *The Applied Dynamics of Ocean Surface Waves*, Advanced Series on Ocean Engineering Vol. 1 (World Scientific Publishing, Singapore, 2003).
- Mei, C. C., Liu, P. L. F., and Ippen, A. T., "Quadratic head loss and scattering of long waves," *J. Waterway, Harbor Coastal Eng. Div.* **100**(WW3), 217–239 (1974).
- Mercier, P. and Guillou, S., "The impact of the seabed morphology on turbulence generation in a strong tidal stream," *Phys. Fluids* **33**, 055125 (2021).
- Monti, A., Omidyeganeh, M., and Pinelli, A., "Large-eddy simulation of an open-channel flow bounded by a semi-dense rigid filamentous canopy: Scaling and flow structure," *Phys. Fluids* **31**, 065108 (2019).
- Morang, A., Rahoy, D. S., and Grosskopf, W. G., "Regional geologic characteristics along the south shore of Long Island, New York," *Coastal Sediments* **1**, 568–583 (1999).
- O'Brien, M. P., "Estuary tidal prism related to entrance areas," *Civ. Eng.* **1**(8), 738–739 (1931).
- O'Brien, M. P., "Equilibrium flow areas of inlets on sandy coasts," *J. Waterway Harbors Div.* **95**(1), 43–52 (1969).
- OGS, "Indagini meteo-oceanografiche, batimetriche, sedimentologiche e morfologiche finalizzate allo studio dei fenomeni di dinamica costiera lungo i litorali di Lignano Sabbiadoro e di Bibione," Technical report No. REL-28/OGA-8 (National Institute of Oceanography and Applied Geophysics, 2004) (in Italian).
- Panuzio, F. L., "The Atlantic coast of Long Island," *Coastal Eng. Proc.* **1**, 222–241 (1968).
- Petti, M., Bosa, S., and Pascolo, S., "Lagoon sediment dynamics: A coupled model to study a medium-term silting of tidal channels," *Water* **10**, 569 (2018).

- Petti, M., Bosa, S., Pascolo, S., and Uliana, E., "An integrated approach to study the morphodynamics of the Lignano tidal inlet," *JMSE* **8**, 77 (2020).
- Petti, M., Pascolo, S., Bosa, S., and Busetto, N., "On the tidal prism: The roles of basin extension, bottom friction and inlet cross-section," *JMSE* **9**, 88 (2021).
- Powell, M. A., Thieke, R. J., and Mehta, A. J., "Morphodynamic relationships for ebb and flood delta volumes at Florida's tidal entrances," *Ocean Dyn.* **56**, 295–307 (2006).
- Rathore, V., Dey, S., Penna, N., and Gaudio, R., "Turbulent flow characteristics over an abrupt step change in bed roughness," *Phys. Fluids* **33**, 095106 (2021).
- Reef, K. R. G., Roos, P. C., Schuttelaars, H. M., and Hulscher, S. J. M. H., "Influence of back-barrier basin geometry on multiple tidal inlet systems: The roles of resonance and bottom friction," *J. Geophys. Res.* **125**(3), e2019JF005261, <https://doi.org/10.1029/2019JF005261> (2020).
- Saville, T., "Sand transfer, beach control, and inlet improvements, Fire Island Inlet to Jones Beach," *Coastal Eng. Proc.* **7**, 785–807 (1960).
- Shin, K. and Hammond, J. K., *Fundamentals of Signal Processing for Sound and Vibration Engineers* (John Wiley & Sons, 2008).
- Stive, M., Ji, L., Brouwer, R. L., van de Kreeke, C., and Ranasinghe, R., "Empirical relationship between inlet cross-sectional area and tidal prism: A re-evaluation," *Coastal Eng. Proc.* **1**(32), 86 (2011).
- Tambroni, N. and Seminara, G., "Are inlets responsible for the morphological degradation of Venice lagoon?," *J. Geophys. Res.* **111**, F03013, <https://doi.org/10.1029/2005JF000334> (2006).
- Umgiesser, G., Canu, D. M., Cucco, A., and Solidoro, C., "A finite element model for the Venice Lagoon. Development, set up, calibration and validation," *J. Mar. Syst.* **51**, 123–145 (2004).
- Umgiesser, G., Helsby, R., Amos, C., and Ferrarin, C., "Tidal prism variation in Venice lagoon and inlet response over the last 70 years," in *Sediment Fluxes in Coastal Areas* (Springer, 2015), Chap. 7, pp. 151–165.
- Umgiesser, G., Sclavo, M., Carniel, S., and Bergamasco, A., "Exploring the bottom shear stress variability in the Venice Lagoon," *J. Mar. Syst.* **51**, 161–178 (2004).
- van de Kreeke, J., "Stability analysis of a two-inlet bay system," *Coastal Eng.* **14**, 481–497 (1990).
- van der Wegen, M., Dastgheib, A., and Roelvink, J. A., "Morphodynamic modeling of tidal channel evolution in comparison to empirical PA relationship," *Coastal Eng.* **57**, 827–837 (2010).
- van Rijn, L. C., "Sediment transport, part III: Bed forms and alluvial roughness," *J. Hydraul. Eng.* **110**(12), 1733–1754 (1984).
- Wolff, M. P., "Natural and man-made erosional and depositional features associated with stabilization of migrating barrier islands, Fire Island Inlet, New York," in *New York State Geological Association Guide Book* (Geology Department, Hofstra University, Hempstead, New York, 1975).